UCRL 3793

UNIVERSITY OF CALIFORNIA

Radiation Laboratory

BERKELEY, CALIFORNIA

DISCLAIMER

UCRL-3793

UNIVERSITY OF CALIFORNIA

Radiation Laboratory
Berkeley, California

Contract No. W-7405-eng-48

NUCLEAR REACTIONS OF COPPER INDUCED BY 5.7-Bev PROTONS

Donald W. Barr

(Thesis)

May, 1957

Printed for the U. S. Atomic Energy Commission

NUCLEAR REACTIONS OF COPPER INDUCED BY 5.7-Bev PROTONS

Contents

NUCLEAR REACTIONS OF COPPER INDUCED BY 5.7-Bev PROTONS

Donald W. Barr

Radiation Laboratory and Department of Chemistry
University of California, Berkeley, California

May, 1957

ABSTRACT

Natural copper was bombarded with 5.7-Bev protons in the University of California Radiation Laboratory's Bevatron. Formation cross sections for 59 radioactive isotopes from mass number 3 (tritium) to mass number 68 (gallium) are reported. The results are quite different from those found at 340 Mev, in that there is an increased tendency to form products removed from the copper target by as many as 40 mass units. On the other hand, the experimentally measured cross sections are similar to those found at 2.2 Bev by workers at Brookhaven National Laboratory. The experimental data were treated empirically, and from the results of this analysis, the cross sections were determined for all stable and unmeasured isotopes with a lower atomic number than copper. A general expression is given, from which any cross section in this study from mass number 22 to 61 may be calculated with a 65% certainty (on the average). The observed distribution of products is discussed in terms of the present ideas on high-energy nuclear reactions, and this distribution is compared to some preliminary theoretical calculations based on a nuclear model that incorporates the above ideas. Observations on the (p,pn) and ($p,p\pi^+$) reactions on copper are compared with those found by other workers at lower energies. The yields of secondary products are discussed.

NUCLEAR REACTIONS OF COPPER INDUCED BY 5.7-Bev PROTONS

I. INTRODUCTION

The study described in this dissertation is typical of the radiochemical type of investigation of nuclear reactions, which has proven to be a very useful means of probing into the properties of the nucleus. It is limited to surveying the end products or debris of the collisions between accelerated particles and heavier target nuclei, but from these observations, information may be deduced concerning the primary events that occurred. The results must be coupled with emulsion and cloud chamber data in which the initial particle-nuclei collisions themselves are studied in order to establish a complete description of the processes involved when nuclear transmutations are induced in a target by particle bombardment.

In recent years, a number of radiochemical studies employing a variety of bombarding particles have appeared in the literature. These encompass a wide range of projectile energies and target materials spread throughout the periodic table. Reasonably complete summaries have recently been compiled.[1-4] Copper has been a particularly popular bombarding material for several reasons:

(a) The pure metal is easily obtained in nearly any desired uniform thickness.

(b) The number of radioactive nuclides that may be formed from the bombardment of copper is not so prohibitively large as to prevent a single experimenter from studying all of the ones with reasonable half-lives, thus obtaining a complete picture of the distribution of products. On the other hand, copper is a sufficiently heavy nucleus (i.e., there are enough elements of lower Z) for one to observe the changes in this distribution over a very wide range of energies.

(c) The radionuclides that can be formed from copper in general have fairly simple decay schemes, and, at this writing, very little ambiguity remains concerning the decay properties of the isotopes included in this study, owing to the very fine cumulative work of nuclear spectroscopists at several laboratories. Well-known decay schemes are essential for accurate cross-section work.

(d) Radiochemical separation procedures are simplified, especially since only the first row of transition elements may be formed from copper.

One disadvantage in bombarding copper is that there are two stable isotopes in natural copper, which complicates the analysis of cross sections for nuclides close to the target.

The bombardment of copper with deuterons,[5-8] alpha particles,[6,7] neutrons,[9] and x-rays,[4] all in the energy range of hundreds of Mev, has shown that the nature of the bombarding particle does not strongly affect the distribution of nuclear products formed, so that the majority of the studies on copper over a wide energy range have employed protons as the projectile. The following is a summary of these radiochemical investigations:

Proton Energy (Mev)	(Worker(s)	Reference
32	Ghoshal	Phys. Rev. 80, 939 (1950)
0-100	Meadows	Phys. Rev. 91, 885 (1953)
49	Carleson	Acta Chem. Scand. 8, 1697 (1954)
90	Coleman, Tewes	Phys. Rev. 99, 288 (1955)
190	Coleman, Tewes	Phys. Rev. 99, 288 (1955)
340	Batzel, Miller, Seaborg	Phys. Rev. 84, 671 (1951)
480	Vinogradov et al.	Conf. Acad. Sciences U.S.S.R. (English translation) p. 85
680	Vinogradov et al.	Conf. Acad. Sciences U.S.S.R. (English translation) p. 85
2200	Friedlander et al.	Phys. Rev. 94, 727 (1954)
5700	Barr	This work

In addition to these rather complete studies, several workers have studied the yields of particular isotopes of interest.[10-12]

For incident particles with energy less than about 50 Mev, the Bohr compound-nucleus model gives an adequate description of observed results.[13] This model pictures the reaction as a two-step process. In a typical event, the incoming projectile is absorbed by a target nucleus to form a compound system, with the kinetic energy of the projectile being distributed among the nucleons during a time which is long compared with the time it would take for the incident particle to traverse the nucleus. During this time, it is assumed that the compound nucleus

"forgets" how it was formed, so that the second step, which is the decay of the system according to various possible modes of particle emission, is independent of the method of formation. The experimental work of Ghoshal has verified this description.

As the bombarding energy is raised, however, the observed results are no longer consistent with the above model, which would predict a rapid decrease in the yields of products close to the original target nucleus. The data of Carleson, Coleman and Tewes, and Batzel show that the majority of the products formed are still close to the target nucleus, but that there is a gradually increasing tendency to form nuclides removed from the copper target by as many as 15 to 20 mass units. The interpretation of these results in terms of a cascade-followed-by-evaporation model is discussed in Section V.

With the advent of very high-energy particle accelerators introducing the onset of meson production, the possibility of new mechanisms led Friedlander and the Brookhaven group to repeat the copper study on the Cosmotron. They found quite different results from those at 340 Mev. The cross sections for products requiring very large amounts of excitation energy had increased by several orders of magnitude, apparently at the expense of those close to the target. With the completion and successful operation of the University of California Radiation Laboratory's Bevatron as the world's highest-energy particle accelerator, it was of immediate interest to extend these measurements for comparison with the previous work and the current ideas on high-energy nuclear reactions. Hence, this study was undertaken.

II. EXPERIMENTAL PROCEDURES

A. Target Arrangements

1. General Foil Stack Content

The targets that were bombarded in the Bevatron consisted of a stack of 3/4-by-1-5/8-inch copper and aluminum foils arranged as shown in Fig. 1 (a). The 3-mil aluminum foil was used to measure the number of protons that had passed through the foil stack by means of the Al^{27} (p,3pn) Na^{24} reaction. For this reason, it is called the beam monitor. A discussion of the cross section for this reaction is given in Section B.

The monitor was preceded by a 1-mil aluminum guard foil in order to compensate for the recoil loss of Na^{24} out of the monitor foil, although this loss can be estimated from published data to be less than 1% for a 3-mil aluminum foil at this energy.[14,15] A 1-mil aluminum guard foil was also inserted between the monitor and the copper target to protect the monitor from impurities due to recoils in the backward direction out of the copper.

The copper target foils varied from 2 to 14 mils thick, depending upon the half-lives of the products to be removed. Since the number of atoms of a nuclide formed during bombardment is proportional to the number of atoms per square centimeter of the target material exposed to the particle beam, an increase in this quantity will lead to more favorable counting rates of the nuclide when it is eventually isolated. This is especially desirable for the longer-lived isotopes. However, for protons in the Bev energy range, there is another factor to be considered, specifically multiple traversals of the target by the proton beam, which is effectively an increase in the beam intensity. A discussion of this effect is given in Section B. The advantage obtained through multiple traversals of the target is enhanced by keeping it as thin as possible. Hence, these two opposing factors were considered when choosing the thickness of copper target material to be bombarded.

2. For Investigating Products Lighter Than Aluminum

For studying those products below aluminum that are formed in the bombardment of copper -- namely Mg^{28}, Na^{24}, and Na^{22}, F^{18}, C^{11}, Be^{7}, and tritium -- it was necessary to guard the copper target from recoils of

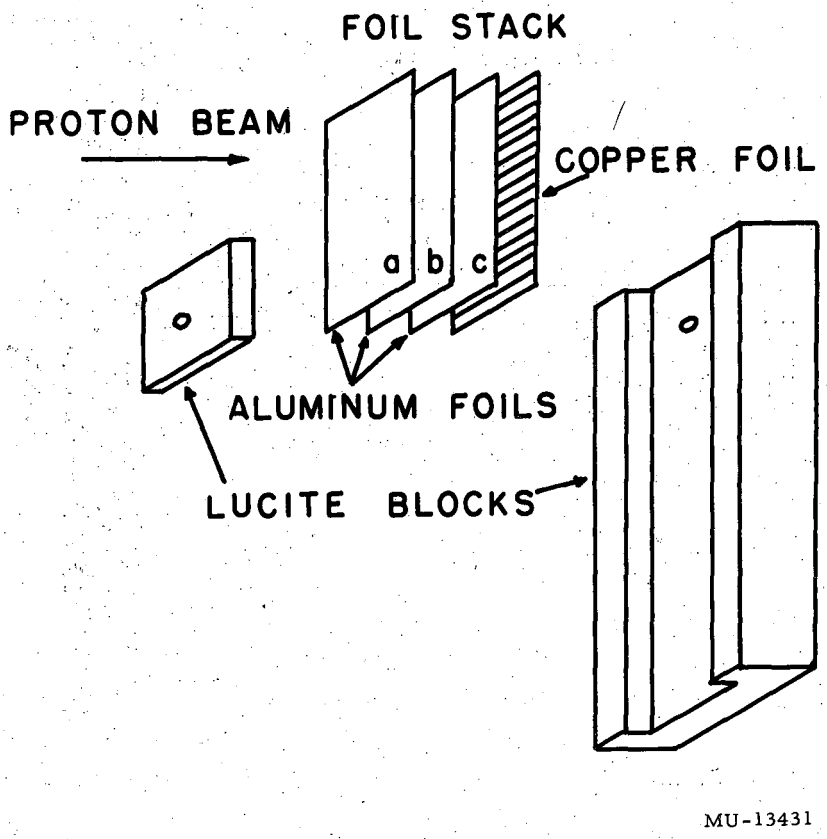

Fig. 1 (a). Details of foil stack and lucite holder; a,c= 1-mil aluminum foils; b= 3-mil aluminum foil.

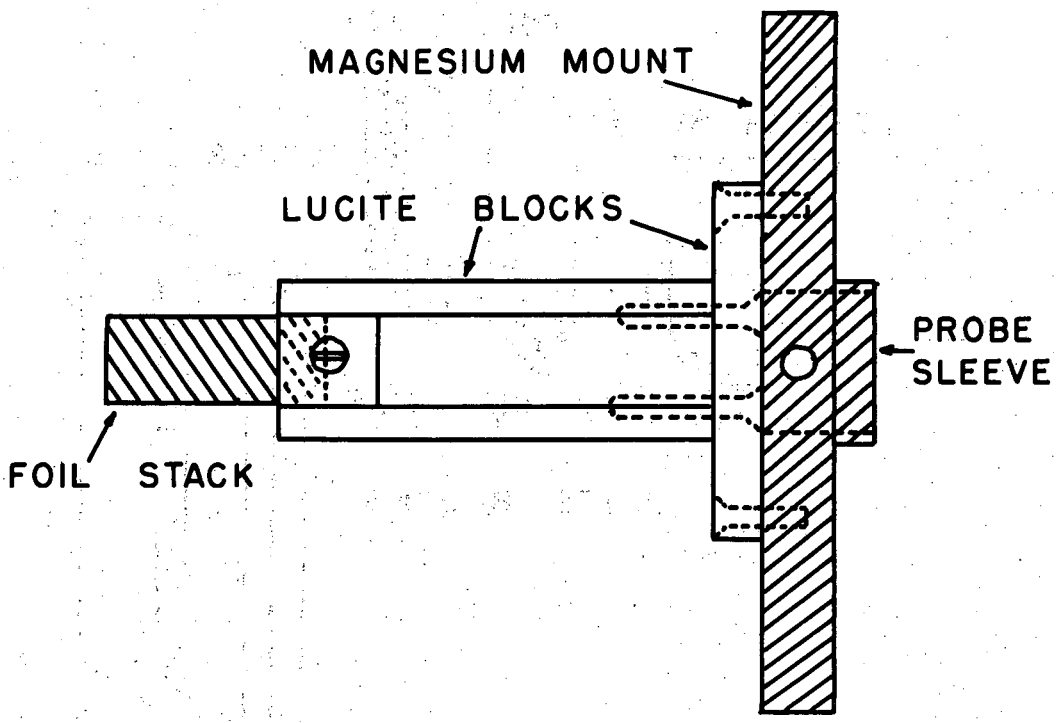

Fig. 1 (b). Complete target assembly.

these same nuclides formed in the aluminum monitor. This was done by placing a copper guard foil before the actual target foil.

3. For Investigating Secondary Products

It was thought that the presence of an aluminum monitor foil giving rise to a flux of low-energy evaporated nucleons might appreciably affect the results for the copper and nickel isotopes. However, the cross sections for the copper isotopes as determined by using the aluminum monitor agreed within experimental error with those obtained by irradiating a bare copper foil and using calcium as an internal monitor. Nevertheless, the zinc and gallium secondary products were studied by using the latter method of internal monitoring, since the formation of these products is especially sensitive to low-energy nucleons.

4. Target Alignment

Since it was critically important to insure that the aluminum and copper foils received the same proton flux during a bombardment, their areas had to be matched as closely as possible when in the foil stack. All foils were machined to the specified dimensions together, and when a target of these foils was being assembled, as much care as possible was taken to align their leading edges with the aid of a magnifying glass. Two small strips of scotch tape placed close to the leading edge were sufficient to keep the foil stack together after a small portion of it had been clamped in the lucite holder shown in Fig. 1 (a). When mounted, the foil stack protruded 1.25 inches beyond the lucite block, and the leading edge of the stack was a total of 5 inches from the face of a magnesium mount to which the lucite was attached, as shown in Fig. 1 (b). The metal mount was provided with a short sleeve which fitted onto the pneumatic probe in the Bevatron. This arrangement was found to be the best for fast removal of the targets from the accelerator. At the conclusion of a bombardment, about 1 inch of the foil stack protrusion was scissored off to be worked up radiochemically.

5. Target Materials

Electrolytic copper foil obtained from A. D. Mackay, Inc. was used as the target material. A spectrochemical analysis revealed a trace of magnesium and silicon (approximately 0.01 to 0.001%), but no other detectable elements. The aluminum foil that was used as the beam monitor contained approximately 0.5% silicon, 0.05% iron, and 0.01% magnesium, as determined by spectrochemical methods. Impurities present in these orders of magnitude make negligible contributions to the activities of isotopes that may be formed from their bombardment, in comparison with the amount formed from the copper or aluminum.

B. Bombardments

1. The Bevatron

A review of proton synchrotrons, to which class of accelerators the Bevatron belongs, and the principles involved in their operation has been given by Livingston.[16] The Bevatron has the so-called "race track" design of four magnet quadrants with straight sections between the quadrants. Its operation depends upon an extension of the synchrotron principle of phase-stable acceleration at constant orbit radius in a magnetic field that increases with time. In addition, since the rotation frequency for protons at constant orbit radius increases by a large factor during acceleration to Bev energies, a variable-frequency accelerating field is also required. Pertinent statistics on the Bevatron in its present state of operation are available in pamphlet form at the University of California Radiation Laboratory (UCRL Pub. No. 2a).

In this study, the major concern was with the proton energy and the beam intensity available. During the early stages of this study, the maximum proton energy was 5.7 Bev. This figure has since risen to 6.2 Bev, but all the experiments mentioned herein were conducted at 5.7 Bev. The beam intensities at first were of the order of 10^9 protons per pulse, with a maximum rate of 12 pulses per minute. Intensities less than this amount would not have been of much use in a study of this sort. However, through improvements, the beam was gradually increased over a period of two years so that 2 to 5 x 10^{11} protons per minute were consistently available, and, just prior to a shutdown at the conclusion of

this work, a beam of 10^{12} protons per minute was obtained. Intensities of this sort made it possible to observe both long- and short-lived isotopes of an element in a single run. As a result, the latter bombardments seldom ran more than 30 minutes.

During the acceleration cycle, the target was withdrawn from the beam aperture. Just prior to the turn-off of the rf acceleration, the target was propelled by means of an air-driven probe to a position slightly smaller than the equilibrium radius of the proton orbit. When the acceleration was turned off, the magnetic field continued to rise, and the proton packet spiraled inwards across the target. The probe was then withdrawn for another cycle.

2. Multiple Target Traversals

Because relatively thin targets were used, it was expected that there would be multiple traversals by the proton beam through the foil stack. This was borne out experimentally by comparing the total number of protons delivered to the target as estimated by a calibrated induction electrode in the Bevatron with the actual number that passed through the stack as obtained from the aluminum monitor foil. The difference between the two estimates was ascribed to multiple traversals, which take place in the portion of the foil stack that protrudes beyond the lucite block described in the last section, since once the proton beam makes a single passage through the thick lucite holder, it is effectively lost thereafter.

In Appendix A, a relation is derived for the number of traversals a proton beam of a given energy makes through a foil stack of any target material. The result for 5.7-Bev protons is

$$\Delta r = \left(0.220 \frac{dE}{dX} b + 0.0003\right) n, \qquad (1)$$

where Δr = length of foil stack through which multiple traversals take place (in inches),

$\frac{dE}{dX}$ = rate of energy loss of protons with target thickness (in Mev per gram per square centimeter),

b = target thickness (in grams per square centimeter),

n = number of traversals.

For the copper-aluminum foil stacks used in this study,

Δr = the 1-inch target protrusion, which was cut off and worked up radiochemically;

for 5.7-Bev protons, $\frac{dE}{dX}_{Cu} = 1.574$ Mev/gram/centimeter^2, (Ref. 17)

$\frac{dE}{dX}_{Al} = 1.782$ Mev/gram/centimeter^2. (Ref. 17)

The variation of the number of traversals with target thickness calculated by insertion of these parameters into Eq. (1) is plotted in Fig. 2 along with the experimental results mentioned previously. The agreement is quite good, and it is probable that Eq. (1) will give accurate results for any target when Δr is of the same magnitude as that used above.

3. Cross Section for Aluminum-27 (p,3pn) Sodium-24

This reaction has been widely used as a beam monitor to measure the number of protons that have passed through a target during a bombardment. This method of monitoring has the advantage that after a 24-hour cooling period, 15.0-hour Na^{24} is the only activity left in the aluminum foil, so that it may then be counted directly. A disadvantage lies in the sensitivity of the reaction to low-energy secondary neutrons, which may form Na^{24} in aluminum by an (n,α) reaction. However, for targets less than a gram per square centimeter, this effect has been shown to be negligible.[18]

Several workers are responsible for the complete excitation function for this reaction from threshold up to 6 Bev.[19-25] In Fig. 3, the most recent results are plotted. Within experimental error, the cross section is constant from 340 Mev to 6 Bev. For this work, 10.5 millibarns was used for the monitor cross section at 5.7 Bev. If a better value for the monitor cross section is obtained in future studies, the experimental cross sections in this investigation can be recalculated.

An alternative reaction, which can be used as a beam monitor for bombardments in the Bev energy range, is Au^{197} (p, spallation) Tb^{149}, which has a threshold of 0.6 Bev, and thus offers the advantage that it is insensitive to low-energy secondary particles. In a suitable counting arrangement, the gold foil may be analyzed directly for the alpha particles from Tb^{149} despite the presence of numerous beta-emitters. The

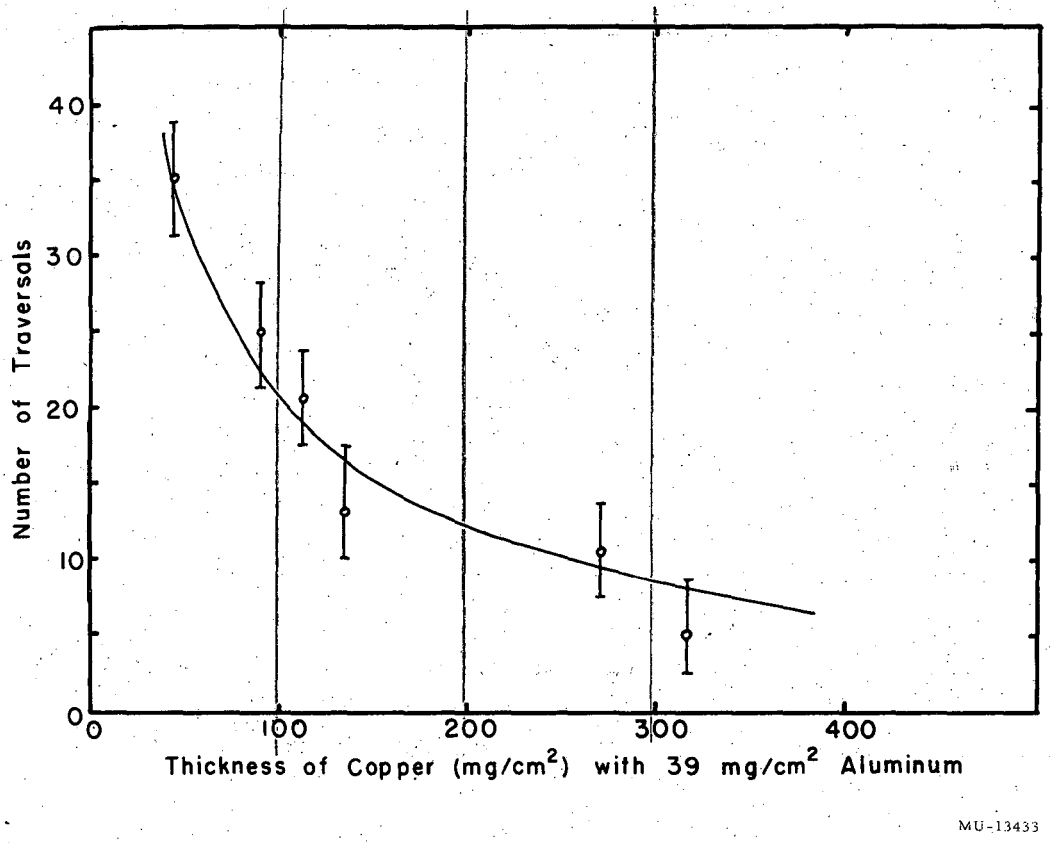

Fig. 2. Multiple traversals of the Bevatron beam through copper targets as a function of the thickness of copper.
o = experimental data; — = calculated from Eq. 1.

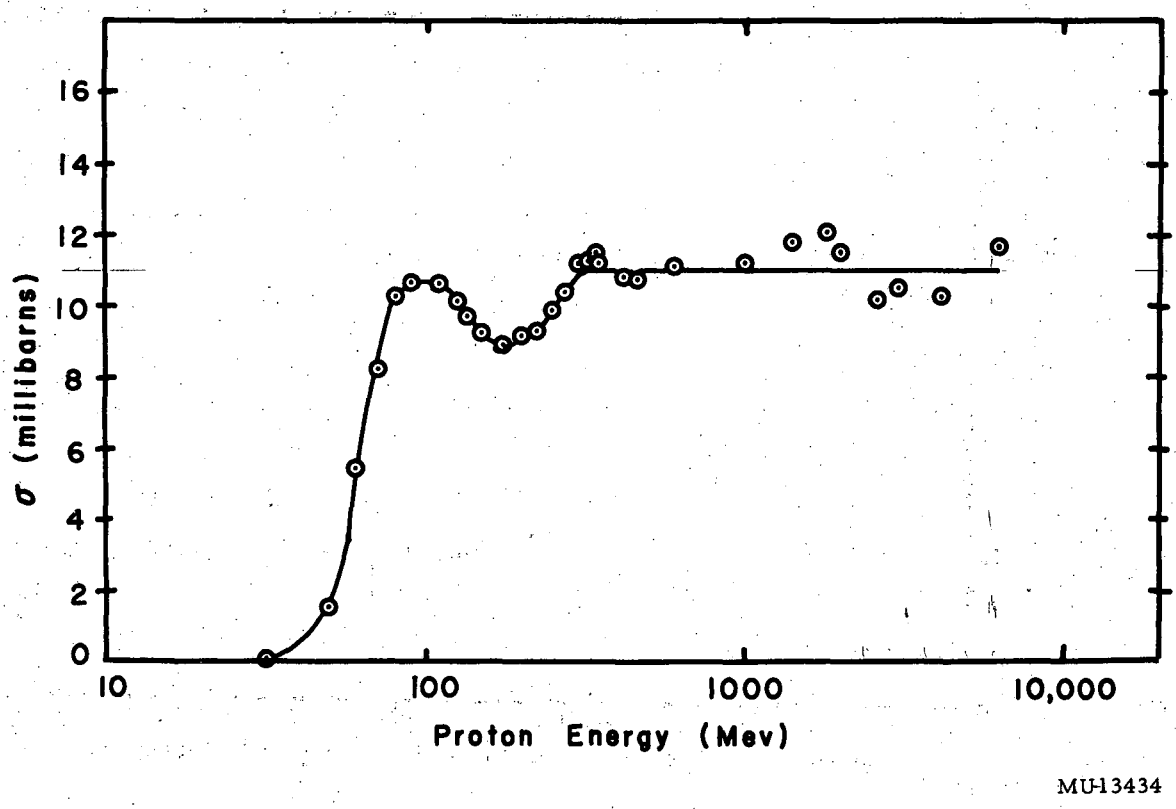

Fig. 3. Complete Al^{27} (p,3pn) Na^{24} excitation function up to 6 Bev.

cross section for this reaction as a function of energy up to 6 Bev has been studied by Duffield and Sugarman[26] and Winsberg.[27]

C. Chemical Separation Procedures

In order to estimate the amount of activity lost through chemical separations of the elements, 1- to 10-milligram amounts of inert carriers of the elements to be removed in a given bombardment were added to the original target solution, usually in the form of chloride or nitrate solutions. Consideration of the gravimetric factor of the eventual weighing form as well as of the energy and type of radiations to be counted governed the exact amount of carrier used in the various bombardments. In most cases this choice was arranged so that eventually the sample lay between 5 and 15 mg/cm^2 in order that an estimate of the self-scattering self-absorption correction described in Section III could be made by using published curves of this correction. In special cases such as S^{35}, Fe^{55}, and V^{49}, where the energy of the radiations is quite low and self-absorption of these radiations in the sample could be significant, samples of less than 5 mg/cm^2 were obtained by using small amounts of these carrier elements. With a known amount of carrier initially added and a chemical yield of the same element in the final precipitate, one has a measure of the amount of activity lost during separations.

The degree of radiochemical purification of an element and therefore the type of chemistry used for its removal depends upon the cross section and counting efficiency of the nuclide under consideration. If these are both high for an isotope, then its degree of purification does not have to be too great, but if they are low, then a good clean separation is necessary. The use of selective gamma-ray analysis appreciably reduces uncertainties of this sort, and indeed, some insight was gained into the chemistry of the elements studied when contamination did occur by establishing unambiguously the nature of the contaminant through gamma-ray analysis and half-life observations. However, an attempt was always made to achieve as high a degree of purification as time allowed by using the techniques of solvent extraction, ion exchange, and selective precipitations. In addition, "holdback" carriers of undesired elements were added to dilute the radioactive species associated

with these elements, and "scavenging agents" were used to remove possible contaminants whose chemistry allowed their precipitation while leaving the desired element in solution.

The following chemical separation procedures are adaptations or revisions of those used by other workers.[28-30] Unless otherwise noted, the copper foils were always dissolved in a minimum of concentrated nitric acid along with the carriers for elements to be removed, and after dissolution, the solution was adjusted to 1N in hydrochloric acid for removal of the copper by addition of hydrogen sulfide.

TRITIUM

The apparatus used to remove tritium is essentially the same as that described by Currie.[18] The copper foil was melted at about 1000° C and allowed to come to equilibrium with hydrogen carrier gas at a pressure of 11 cm mercury in a quartz furnace tube (volume approximately 0.1 liter). The gas was then passed through a palladium thimble and into a counting tube, which had previously been filled with a little less than an atmosphere of methane as the counting gas. The chemical yield was 38%.

BERYLLIUM

Ten milligrams of beryllium carrier was used. The element was first removed as the hydroxide with ammonia. The precipitate was dissolved in hydrochloric acid, ferric ion was added, and the solution was nearly neutralized with sodium hydroxide. It was then transferred with vigorous stirring to another cone containing enough 20% sodium hydroxide to give the whole solution a 5% base concentration. After digestion of the precipitate, the ferric hydroxide was centrifuged and removed. The iron scavenging was repeated. The supernate containing the amphoteric beryllate ion was neutralized, and the hydroxide was again precipitated with ammonia. It was dissolved in 3N sodium hydroxide, a saturated ammonium chloride solution was added, and the mixture was digested to reprecipitate beryllium hydroxide, which was centrifuged, washed, and then redissolved in hydrochloric acid. About 15 cc of a pH6 sodium sulfite-bisulfite buffer was added. The beryllium was extracted into

an equal volume of a 0.4M thenoyltrifluoroacetone (TTA) in benzene solution by rapid equilibration for 20 minutes. The organic phase was then washed successively with: water twice; 8M nitric acid twice; water once; 1N sodium hydroxide twice, NOT LONGER THAN 10 SECONDS FOR EACH WASH; once quickly with water. Beryllium was then re-extracted into a 2:1 mixture of concentrated formic: concentrated hydrochloric acid, from which the hydroxide was precipitated with ammonia after neutralization. After the precipitate was washed and dried, it was ignited at 1000° C to beryllium oxide, and weighed. Chemical yields were 50% to 60%.

CARBON

See argon procedure.

FLUORINE

Ten milligrams of fluorine as ammonium fluoride was added to the target solution. Calcium fluoride was precipitated by the addition of an excess of calcium nitrate solution and enough ammonia to make the mixture alkaline. The precipitate was washed with water and transferred to a distilling flask, and 72% perchloric acid was added. Fluosilicic acid (the silicon was supplied by the glass walls of the vessel) was distilled out at 130-160° C, and the distillate was caught in a pH 6 acetate-buffered lead chloride solution to precipitate lead chlorofluoride. This was then transferred to a second distilling flask, and the above distillation with perchloric acid was repeated. The distillate from this step was caught in a neutral solution of calcium nitrate to precipitate the fluorine finally as calcium fluoride, which was filtered, dried, and weighed in this form for the yields of fluorine. These ran about 20%.

SODIUM

Ten milligrams of sodium carrier was used. The target solution, adjusted to concentrated hydrochloric acid, was cooled in an acetone-ice bath, and anhydrous hydrogen chloride gas was passed through for 15 minutes to precipitate sodium chloride. The salt was washed with two small portions of concentrated hydrochloric acid saturated with gas. It was dissolved in water and scavenged with ferric hydroxide by addition

of ammonia, and the ammonium ion was destroyed by heating with aqua regia. A reprecipitation of sodium chloride was carried out. After the precipitate was washed as above, the salt was transferred with absolute alcohol to a weighed platinum plate, dried with a heat lamp, and weighed as sodium chloride. Chemical yields were of the order of 20% to 30%.

MAGNESIUM

Five milligrams of carrier was used. Magnesium was removed as the carbonate from the supernate after removal of the acid and basic sulfides. The magnesium carbonate was washed and then dissolved in dilute acetic acid, and a calcium scavenging was performed with saturated oxalic acid. The oxalate ion was destroyed by boiling with concentrated nitric acid. The solution was then neutralized with ammonia and made just acidic with dilute hydrochloric acid. Upon addition of a saturated solution of diammonium phosphate, magnesium was precipitated; it was washed with dilute ammonia. The hydrated magnesium ammonium phosphate was ignited at 1300° F to magnesium pyrophosphate for weighing. Chemical yields were about 50%.

SILICON

Ten milligrams of silicon was added to the target solution in the form of ammonium fluosilicate. The element was precipitated as the hydrated oxide after addition of boric acid to complex the fluoride ion and digestion of the target solution with concentrated sulfuric acid. The gel was washed with dilute sulfuric acid, and it was redissolved by the addition of potassium hydroxide solution. Two titanium scavengings were performed on the basic solution, and holdback carriers for the other elements were added. The solution was acidified with hydrochloric acid, and then digested to reprecipitate the hydrous oxide. The whole procedure was repeated from the dissolution with potassium hydroxide, and the final silica precipitate was ignited at 625° C to silicon dioxide for weighing. Yields were about 50%.

PHOSPHORUS

Five milligrams of carrier as phosphate ion was used. The target solution was nearly neutralized with ammonia and adjusted to 2N in nitric acid. The phosphorus was precipitated from this solution by the addition of an excess of ammonium molybdate reagent and digested at 50° C. The ammonium-phosphomolybdate precipitate was washed and redissolved in hot concentrated ammonia containing a little citric acid to complex titanium. Vanadium and titanium holdbacks were added, and most of the ammonia was neutralized with hydrochloric acid. Sulfur dioxide was then bubbled through the solution to reduce vanadium from its pentavalent to its quadrivalent state, in which condition it does not coprecipitate with phosphorus when the latter is brought down by the addition of magnesia mixture. The phosphorus was then precipitated as magnesium ammonium phosphate by the addition of cold magnesium chloride reagent and enough ammonia to make the solution strongly alkaline. Cooling in an ice bath aids more complete recovery of the phosphorus. The precipitate was dissolved in hydrochloric acid, and a reprecipitation of magnesium ammonium phosphate was performed. The sample was eventually ignited at 1300° F to magnesium pyrophosphate for weighing. Chemical yields ran close to 80%.

SULFUR

Two milligrams of sulfur as sulfate ion was added as carrier. The sulfate was precipitated as its barium salt from the target solution adjusted to 1N in hydrochloric acid, and it was washed well with small portions of water. The barium sulfate was slurried with a concentrated solution of potassium carbonate while being heated in a water bath for about an hour. Barium was converted to the carbonate by this treatment, leaving sulfate in solution. The metathesis of the barium carbonate was repeated in order to regain as much sulfate as possible. The supernates were combined, carefully neutralized with hydrochloric acid, and adjusted to 1N with respect to acid. Carbon dioxide was expelled by heating, and sulfate reprecipitated with addition of excess barium chloride solution. The whole procedure was repeated from the potassium carbonate metathesis, and barium sulfate was finally dried and weighed in order to obtain the chemical yield of sulfur, which was about 50%.

CHLORINE

Five milligrams of chlorine as sodium chloride was placed in a small distilling flask along with the target foil. Enough concentrated nitric acid to dissolve the foil completely was added quickly, and the system immediately closed. The flask had provisions for passing a gentle stream of air continually through the target solution in order to enhance the passage of liberated gases into the receiving cone, which contained about 3 cc of water made strongly basic with potassium hydroxide. It also contained hydrogen peroxide in order to insure catching the chlorine whether it came over as hydrogen chloride or as molecular chlorine. The flask was heated rapidly for a few minutes after complete dissolution of the target foil. The receiving vessel was then removed, and the solution was acidified with nitric acid. Chloride ion was precipitated by the addition of excess silver nitrate and digestion in a hot-water bath to aid coagulation of the silver chloride. The centrifuged precipitate was washed with dilute nitric acid, and then it was dissolved in concentrated ammonium hydroxide. A ferric (nitrate) scavenging was performed on the basic solution, and nitric acid was added to acidify the supernate. Silver chloride precipitated from the acid solution, and excess silver ion was added to insure complete precipitation. After this final step, the silver chloride was not digested to induce coagulation, but filtered immediately. This gave much smoother samples of silver chloride, which were then dried and weighed for the yields of chlorine, which were 30% to 40%.

ARGON

The argon experiment was carried out in the UCRL Chemistry Department's tritium apparatus, and because a good technique for purifying the argon chemically would have entailed revising the vacuum line somewhat, only two steps were taken to prevent contamination by possible impurities: (1) a room-temperature activated-charcoal trap was placed at the mouth of the furnace tube; (2) the argon sample was passed through a liquid-nitrogen-cooled finger in an attempt to freeze out the argon, with the intent of then letting it distill out as the finger was slowly warmed, leaving less volatile impurities such as carbon dioxide behind. The latter step proved ineffective, probably

because the gas was passed through the finger too quickly. However, the only impurity observed in the argon sample was C^{11}, whose half-life fortunately is short enough so that the data on argon were useful. As in the tritium procedure, the copper foil was melted in a furnace tube which contained argon gas at 10 cm mercury as carrier. The chemical yield was 47%.

POTASSIUM

Ten milligrams of potassium was used as carrier. After removal of the acid and basic sulfides, calcium and magnesium were precipitated as carbonates. Ammonium ion was destroyed by heating the potassium supernate to dryness several times with nitric acid. The salt was dissolved in a minimum amount of water, and about 5 cc of concentrated perchloric acid was added. Potassium perchlorate precipitated when the solution was cooled in an ice bath. The centrifuged precipitate was redissolved in 1 cc of perchloric acid with heating to 90° C. Potassium perchlorate was brought down again in an ice bath. The reprecipitation was repeated three times, and the final sample was washed with absolute alcohol and dried under a heat lamp to be weighed as potassium perchlorate. Chemical yields were about 40%.

The above procedure consistently failed to remove about 0.5% by activity of phosphorus impurity -- which does not affect the potassium results, however, because of the comparative half-lives involved. Partly because of this impurity, but mostly in order to observe short-lived K^{38} and K^{44}, a much faster chemical procedure was tested, with good results. This involved precipitation of potassium tetraphenyl boron, which is a fine white salt. Two milligrams of carrier is sufficient, and the precipitation can be carried out from the target solution adjusted to about 15 cc volume with a pH of 4 to 5 and warmed to 40° C. The reagent used is a 0.1 M solution of sodium tetraphenyl boron obtainable from the Matheson Chemical Company. An excess of the reagent should be avoided during precipitation, since it tends to co-precipitate with the potassium salt. The procedure is reported to remove potassium cleanly from all the alkaline earth and transition elements,[31] although cesium, rubidium, and ammonium ions are also

precipitated. However, for removing potassium from copper, the method seems ideal for looking at the short-lived isotopes mentioned, although — owing to an accelerator shutdown toward the end of this study — it was never actually tested on a bombardment.

CALCIUM

Five milligrams of calcium carrier was added. The acid and basic sulfides were removed, and the calcium supernate was heated to drive off hydrogen sulfide. The solution was acidified with oxalic acid, and calcium was precipitated by the addition of ammonium oxalate and digestion in a water bath. The hydrated calcium oxalate was dissolved in dilute nitric acid, and oxalate ions were destroyed by boiling the solution rapidly with potassium chlorate present. The solution was made basic with ammonia, and two ferric scavengings were performed. Oxalic acid was added to acidify the supernate, and calcium oxalate was reprecipitated. It was washed with small portions of water and dried at 110° C to be weighed. Chemical yields were 60% to 70%.

SCANDIUM

Ten milligrams of scandium carrier was used. The element was first precipitated as the hydroxide with ammonia after removal of the copper. The hydroxide was dissolved in concentrated hydrochloric acid, titanium (IV) and ferric holdbacks were added, and the solution was passed through a pretreated Dowex A-1 ion-exchange column (200–400-mesh resin). Scandium does not exchange with this resin, and it eluted quickly. The hydroxide was again precipitated with ammonia, and it was washed with dilute ammonia. It was dissolved in 0.1 N hydrochloric acid, and the solution was carefully adjusted by means of a meter to a pH of 2.0 with dilute hydrochloric acid and sodium hydroxide. Scandium was extracted into an equivalent volume of 0.4 M thenoyltrifluoroacetone (TTA) in benzene by equilibrating the phases for ten minutes. The organic phase containing scandium was removed and washed well with small portions of water. Scandium was re-extracted into two 3-cc portions of 1 N hydrochloric acid, and it was finally precipitated as the hydrous

oxide with sodium hydroxide. The analysis was done colorimetrically with alizarin red as the complexing agent. Chemical yields were 30% to 50%.

TITANIUM

Five milligrams of titanium (IV) carrier as titanic acid was added. The first precipitation of titanium was as the hydroxide, which was washed and then dissolved in hydrochloric acid. Tartaric acid was added to complex the titanium, and an iron-manganese basic sulfide scavenging was performed. The supernate containing titanium was made 1 N in hydrochloric acid, and the cupferrate was formed by the addition of 6% aqueous cupferron reagent. The titanium cupferrate was then extracted into chloroform, and the organic layer was washed with 1 N hydrochloric acid. After evaporation of the organic layer over concentrated nitric acid to destroy all organic matter, the residue was taken up in acid and made alkaline to precipitate titanium hydroxide again. This was dissolved in 6 N nitric acid, and potassium titanium iodate was brought down by the addition of 0.5 N potassium iodate. The precipitate was dissolved in hydrochloric acid and sodium sulfite, and titanium was brought down finally as the hydroxide for mounting. The analyses were done colorimetrically, using the peroxide complex in sulfuric acid solution. Yields were about 30%.

VANADIUM

Two to five milligrams of vanadium (V) carrier as vanadic acid was used. The removal of copper sulfide was performed in the presence of tartaric acid to complex the vanadium. Hydrogen sulfide was boiled out of the supernate, which was then adjusted to about 20 cc of 1 N hydrochloric acid solution. Vanadium and iron were extracted as cupferrates, with 1% aqueous cupferron reagent, into successive 10-cc portions of chloroform. The organic layer was washed with 1 N hydrochloric acid, and it was then evaporated to dryness over concentrated nitric acid to get rid of all organic matter. The residue was dissolved in hydrochloric acid, and titanium carrier was added. The solution was made alkaline with sodium hydroxide, and the hydroxides of iron and titanium were removed. The supernate was made just acidic with acetic acid, and lead

vanadate was precipitated by the addition of a 10% solution of lead acetate. It was normally mounted and weighed in this form except when data on V^{49} were desired. In the latter case, the lead vanadate was dissolved in 2 N nitric acid, and the lead was precipitated with hydrogen sulfide. The gas was expelled and the solution was evaporated to dryness, whereupon the sample was ignited to vanadium pentoxide for mounting and x-ray counting. Yields were close to 80%.

CHROMIUM

Ten milligrams of chromium (VI) as dichromate was used as carrier. The copper was removed from 1 N hydrochloric acid with hydrogen sulfide, during which step the chromium is reduced to the trivalent state. It was then precipitated, along with the other basic sulfides, by the addition of ammonia and additional hydrogen sulfide. The sulfides were dissolved in concentrated nitric acid, free sulfur was removed, and the solution was made up to 5 cc with fuming nitric acid, after which manganese was precipitated as the dioxide by the addition of solid potassium chlorate and heating. During this step, chromium is reoxidized to the hexavalent state. The solution, containing the chromium and holdbacks of the other remaining elements, was adjusted to 1 N in nitric acid and cooled in an ice bath. Four cc of cold diethyl ether was added, and, with constant stirring, a few drops of hydrogen peroxide were introduced. The blue peroxychromic acid was extracted into the ether layer, and the extraction was repeated with an additional portion of ether. The combined organic phases were washed with water acidified with nitric acid. The ether layer was evaporated over a 0.5 N sodium hydroxide solution, and, after acidification with acetic acid, barium chromate was precipitated by the addition of 0.4 M barium chloride solution. It was weighed in this form for the yields of chromium, which ranged from 20% to 80%.

MANGANESE

Ten milligrams of manganous ion was added as carrier. Copper was removed as the sulfide, and, with tartaric acid present to complex vanadium and titanium, the solution was made alkaline with ammonia to precipitate the basic sulfides, including manganese. These were

dissolved in concentrated nitric acid, elemental sulfur was removed, and the solution was brought to 5 cc with fuming nitric acid. Manganese dioxide was precipitated by the addition of small portions of solid potassium chlorate while the solution was heated in a water bath. The precipitate was dissolved in a minimum amount of concentrated nitric acid and hydrogen peroxide. Holdback carriers for adjacent elements were added, and manganese dioxide was again precipitated from a fuming nitric acid solution. The procedure was repeated again when time allowed. Analyses were done colorimetrically on permanganic acid. Yields ran close to 80%.

IRON

Five milligrams of ferric ion was added as carrier. The target solution was adjusted to 7.7 N hydrochloric acid, and the iron was extracted into isopropyl ether. The ether layer was washed well with 7.7 N acid, and then it was evaporated over water on a hot plate. The solution containing the iron was made basic with sodium hydroxide, and ferric hydroxide was centrifuged after digestion. The precipitate was dissolved in hydrochloric acid, and the extraction was repeated. Analyses were done volumetrically. Chemical yields were better than 75%.

COBALT

Five milligrams of cobaltous ion carrier was used. Copper was removed, and cobalt was precipitated along with the other basic sulfides after the addition of ammonia and additional hydrogen sulfide. The sulfides were dissolved in 6 M hydrochloric acid and solid potassium chlorate. The solution was adjusted to 3 N in acetic acid, and cobalt was precipitated by the slow addition of 3 cc of a hot, saturated potassium nitrite solution acidified with acetic acid. The potassium cobaltinitrite was digested in a water bath, and, after centrifugation, it was washed with an acidified 5% potassium nitrite solution. It was dissolved in hydrochloric acid, holdbacks for neighboring elements were added, and a reprecipitation was carried out. Potassium cobaltinitrite was weighed for the yields of cobalt, which were 60% to 80%.

NICKEL

Five milligrams of nickel carrier was added. After removal of copper sulfide, the supernate was boiled to remove hydrogen sulfide, and then it was made ammoniacal to precipitate hydroxides of the transition elements not forming ammonia complexes. The precipitate was washed with hot ammonium chloride solution, and the wash was added to the supernate containing nickel in the form of its ammonia complex. A ferric-ion scavenging was performed on the basic solution. After acidification with acetic acid, nickel was precipitated by the addition of a slight excess of a 1% alcoholic solution of dimethyl gloxime. The nickel precipitate was washed with water, and it was dissolved in concentrated hydrochloric acid. Cobalt and manganese holdbacks were added, the solution was neutralized with ammonia, and it was made just acidic with acetic acid to reprecipitate nickel, which was weighed as the dimethylglyoxime salt. Chemical yields were 40% to 50%.

COPPER

The dissolved target foil acted as carrier for the copper activities. The target solution was adjusted to 1 N hydrochloric acid, and solid sodium bisulfite was added to reduce cupric to cuprous ion. A portion of the copper was then precipitated as thiocyanate by the addition of a few drops of 3 M sodium thiocyanate. The cuprous thiocyanate was washed with water and dissolved in nitric acid. The solution was adjusted to 1 N acid, after boiling with concentrated hydrochloric acid to remove nitrate, and cuprous thiocyanate was precipitated as before. It was weighed in this form. This procedure permits short-lived Cu^{60} and Cu^{62} to be seen easily. If only Cu^{61} and Cu^{64} are to be studied, the precipitation of copper sulfide first leaves the target solution in a more favorable condition for removal of other elements.

ZINC

Five milligrams of zinc was added as carrier. Copper sulfide was removed, and zinc was precipitated along with the other basic sulfides. The precipitate was dissolved in hydrochloric acid and

potassium chlorate, and the solution was adjusted to about 6 N acid. The solution was then put on a pretreated Dowex-1 anion-exchange column. Zinc exchanges with the resin, and it remains down to hydrochloric acid molarities below one, while all other exchanging elements -- such as cobalt, iron, and gallium -- are eluted by a 1.5 M acid concentration. The resin was washed well with 1.5 M acid, and zinc was finally eluted with pure water. The eluate containing the zinc was adjusted to 1 N hydrochloric acid, and 1 cc of saturated oxalic acid was added. The zinc was precipitated by addition of an excess of ammonium thiocyanate and mercurous chloride reagent, with cooling in an ice bath. Scratching the sides of the container also aids in inducing precipitation. The zinc mercuric thiocyanate was dried for 10 minutes in a vacuum desiccator, and weighed for the chemical yields of zinc. These were greater than 70%.

GALLIUM

Five milligrams of gallium carrier was added. The target solution was adjusted to 7.7 N hydrochloric acid. Gallium and iron were extracted into isopropyl ether, and the organic layer was washed with 7.7 N acid. The organic phase was evaporated over water on a hot plate. The water solution of gallium and iron was adjusted to 1 N in sodium hydroxide, and was digested to precipitate ferric hydroxide. An additional iron scavenging was performed on the basic solution. The gallium supernate was adjusted to 7.7 N hydrochloric acid, and the ether extraction was repeated. The gallium was finally precipitated as the 8-hydroxyquinolate by the addition of a slight excess of a 0.35 M aqueous solution of 8-hydroxyquinoline made 2 N with respect to acetic acid, and by the subsequent slow addition of 6 M ammonium acetate until the permanent yellow precipitate formed. One cc excess of reagent was then added and the solution warmed to about 60° C. The gallium 8-hydroxyquinolate was dried at 110° C, and was weighed for the yield of gallium, which was 65%.

D. Counting Techniques

1. Mounting of Samples

The final precipitates were filtered onto previously tared filter paper by use of the chimney setup shown in Fig. 4(a). The filters were standard 7/8-inch-diameter disks bored out of a stack of No. 42 Whatman filter papers by means of a cork borer mounted in a lathe. Prepared in this manner, the filter disks seldom varied more than a milligram from an average weight. After being dried and weighed for the chemical yields, the samples were mounted on strips of two-sided scotch tape which were adhered to standard 3.5-by-2.5-inch indented aluminum cards (350 milligrams per square centimeter). A thin covering of rubber hydrochloride (0.6 mg/cm^2) was stretched over each sample and attached around the filter to the uncovered portion of the scotch tape strip, as illustrated in Fig. 4(b). This arrangement kept the samples firmly in place even over many months of counting.

The aluminum monitor foil was cut into two pieces, which were mounted on separate cards for counting to insure that none of the Na^{24} activity in the foil would be missed because of a sample size larger than the counter window. No sample cover was necessary for these foils.

Samples for which the rate of emission of x-rays was to be determined were mounted on small aluminum hats with a zapon film and left uncovered. Since the energy of aluminum x-rays is well below that for the transition elements, they would not interfere with the counting of these elements in case the radiations emanating from the samples induced x-rays in the aluminum mount.

2. Description of Instruments Used

Four types of instruments capable of detecting the various radiations associated with the decay of nuclear species were used in this study. The following is a brief description of each of these counters:

(a) Geiger counter; beta-particle counting. In the very early stages of this work, argon-filled, chlorine-quenched Geiger tubes with a 3-mg/cm^2 mica end window were in use at this laboratory for counting beta radiations. A small portion of the data was obtained on these counters.

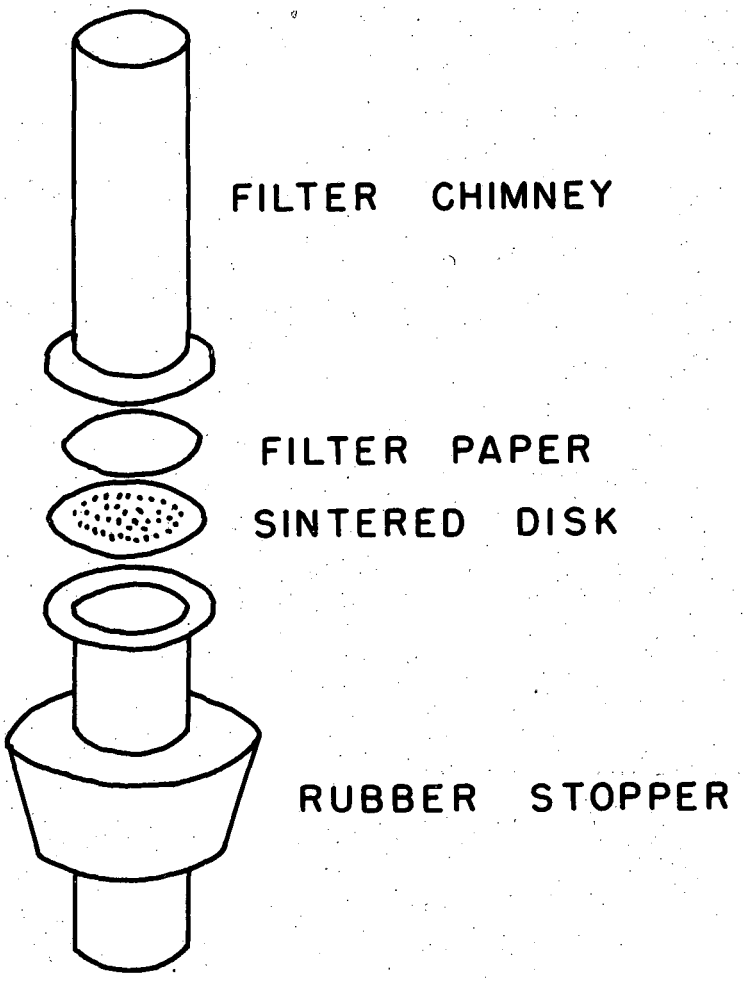

Fig. 4(a). Mounting of sample on filter paper.

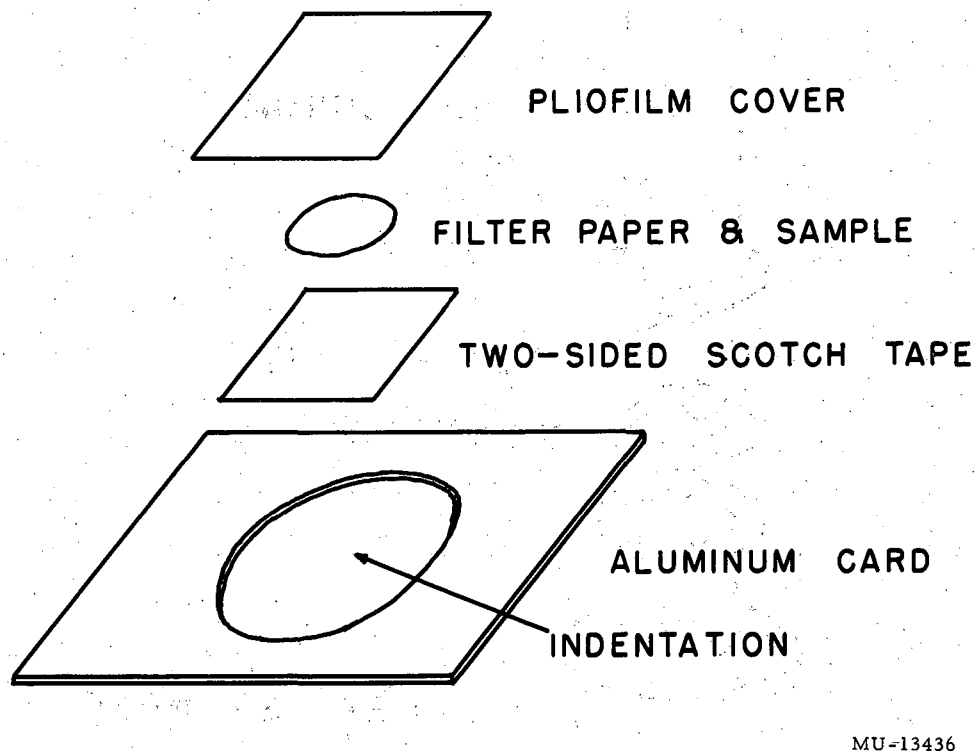

Fig. 4(b). Mounting of sample for radiation measurements.

(b) Proportional counter; beta-particle counting. End-window, methane-flow proportional counters have since replaced the Geiger tubes mentioned above. Several advantages have resulted from this change, among them increased stability and higher geometry obtainable. A 2-mil-diameter tungsten wire is used as the high-voltage and collector electrode. The window is made of aluminized mylar 1 mg/cm^2 thick and 1 inch in diameter. A notched aluminum sample holder permits a mounted sample to be placed at any one of nine distances from the window, corresponding to different geometries. These counters are used in conjunction with a fast linear amplifier and the common scaling unit employing powers of two as a scaling ratio. Tests made with high-energy (Na^{24}) and low-energy (Co^{60}) beta-emitting standards on these counters indicated that there was no sensitive-volume discrimination on any shelf over this range of beta energies.

(c) Windowless proportional counter; x-ray counting. For two of the isotopes studied, Fe^{55} and V^{49}, the absence of beta and gamma radiations necessitated the counting of x-rays in the 5-kilovolt region. A windowless, 90% argon-10% methane gas-flow proportional counter and pulse-height analyzer were used for this purpose.

(d) Sodium iodide scintillation spectrometer; gamma-ray counting. For the extensive gamma-ray counting that was done, a sodium iodide (thallium activated) crystal, 1.5 inches in diameter by 1 inch high, was used in conjunction with the 50-channel differential pulse-height analyzer mentioned above. The crystal was encased with a coating of magnesium oxide and separated from the sample being counted by a thin beryllium window. A quartz disk bonded to the crystal was optically coupled to a Dumont 6292 photomultiplier tube. Counting rates were limited by the dead time of the mechanical registers (40 milliseconds/channel), but this was not a severe restriction for samples obtained in Bevatron bombardments. Quite recently, the analyzer described has been replaced by a 100-channel fast type, of Los Alamos design, available commercially from the Pacific Electro-Nuclear Company (PENCO). All four counters were surrounded by appropriate lead housings to reduce background and isolate the samples during counting. When the samples were counted, a compromise was always struck between the accumulation of

sufficient statistics to insure an accurate counting rate and the minimizing of the counting time relative to the half-life involved, so that the mid-time of the count could be taken to represent the activity determined over the interval.

III. TREATMENT OF DATA

A. Analysis of Decay Curves

1. Graphical Analysis

When more than one isotope was present in a sample, which was generally the case, it was necessary to determine the fractions of the total observed activity that were associated with these various isotopes. It was often possible to select and study a specific gamma ray in the decay of an isotope in the scintillation spectrometer, but for following the decay of particulate radiation on a proportional counter, the overall curve had to be resolved into the separate contributions. This is usually done by observing the decay until only the component of longest half-life remains, and its counting rate is then accurately known. The activity due to this isotope can be calculated at any time during the counting period from a knowledge of its half-life and use of the first-order rate law, which is always obeyed in the decay of nuclear species and subsequently subtracted from the gross activity at that time. The isotope of next longest half-life may then be similarly treated, and the process repeated until all the activity observed over the whole counting period is attributed to one or another of the isotopes originally present. The analysis may be performed graphically on semilog paper, or mathematically, using the decay law and known half-lives for the isotopes. The latter method is somewhat more time-consuming, but was used exclusively in this study when it was shown to give much more reproducible results than the graphical method. However, when there are several isotopes of similar half-life present, as in scandium formed from copper, decay-curve analysis of the beta-particle counting data is very difficult, and selective gamma-ray counting is necessary for

accurate results. Figures 5(a) and 5(b) show the proper decay-curve analysis of a scandium sample obtained in this work and counted in a proportional counter. The actual counting rates of the individual components were obtained by gamma-ray analysis with subsequent conversion to beta-particle rates by means of the factors discussed in Section B. It can be seen that decay-curve analysis of the gross counting data would probably not have yielded very accurate results except for long-lived Sc^{46}.

2. Least-Squares Analysis

In some samples, an unfortunate combination of yields (number of atoms formed) and half-lives of the isotopes led to an apparent decay intermediate to those of its components, and the gross decay curve dropped to a null counting rate without ever showing sufficient curvature to allow a decay-curve analysis to be applied. One example in this study was the element phosphorus, which has radioactive isotopes of mass numbers 32 and 33 whose half-lives are 14 and 25 days respectively, with the yields favoring the former by about 3.5 to 1. The gross decay curve of one of these samples, shown in Fig. 6, has only a very slight curvature and an apparent half-life of 16 to 17 days. In cases of this sort, the activities at the end of the bombardment are most accurately obtained by employing the method of least squares to this complex decay. The equations for the application of this method of analysis to a two-component decay system are worked out and presented in tabular form for convenient use in Appendix B. The extension of the least-squares fit of decay data to more than two components is not difficult, but the amount of labor involved increases rapidly. The results of this type of analysis for the P^{32}-plus-P^{33} example mentioned above is included in Fig. 6. Other cases in this study in which it was necessary to utilize this method to resolve activities were: K^{42} and K^{43}; Ca^{47} and Sc^{47} daughter; Mn^{52m} and Mn^{51}; Cu^{62} and Cu^{60}. In these cases, either the lack of gamma rays, low counting rates, or short half-lives prohibited the use of the gamma-ray spectrometer for resolution.

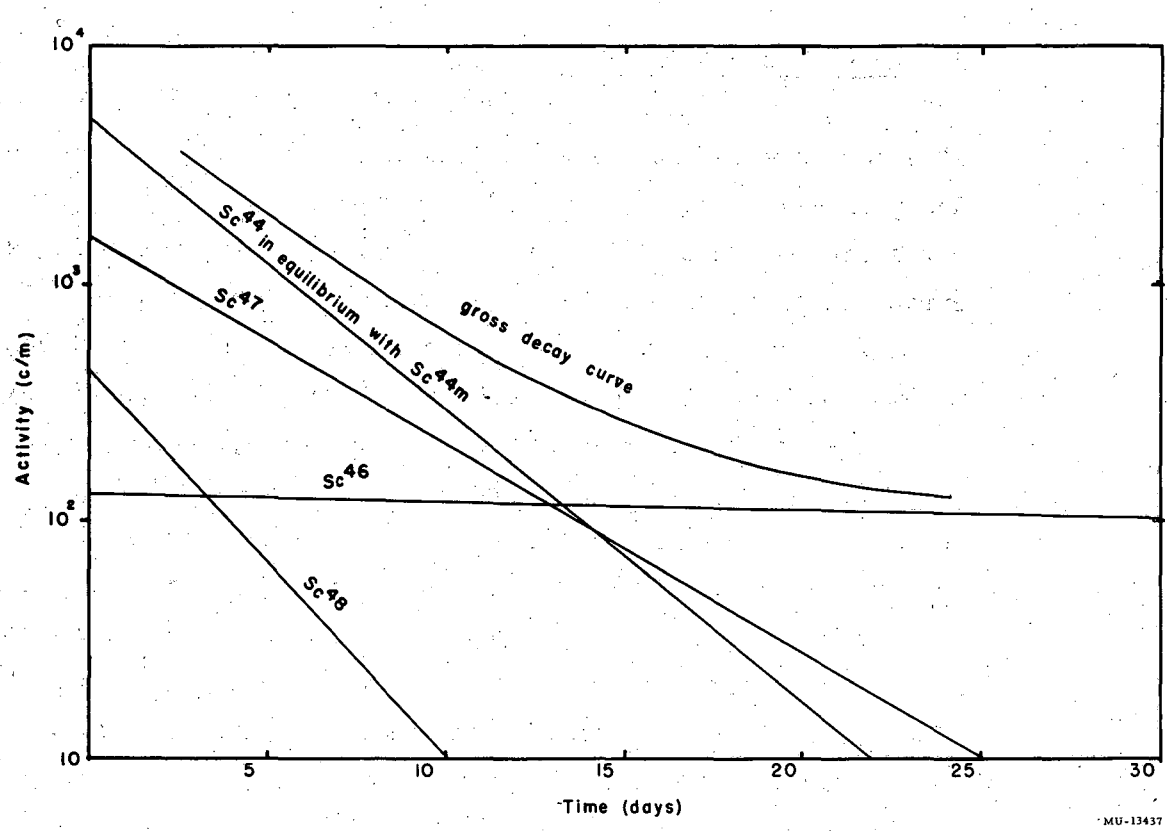

Fig. 5(a). Proportional-counter decay-curve resolution of long-lived scandium isotopes.

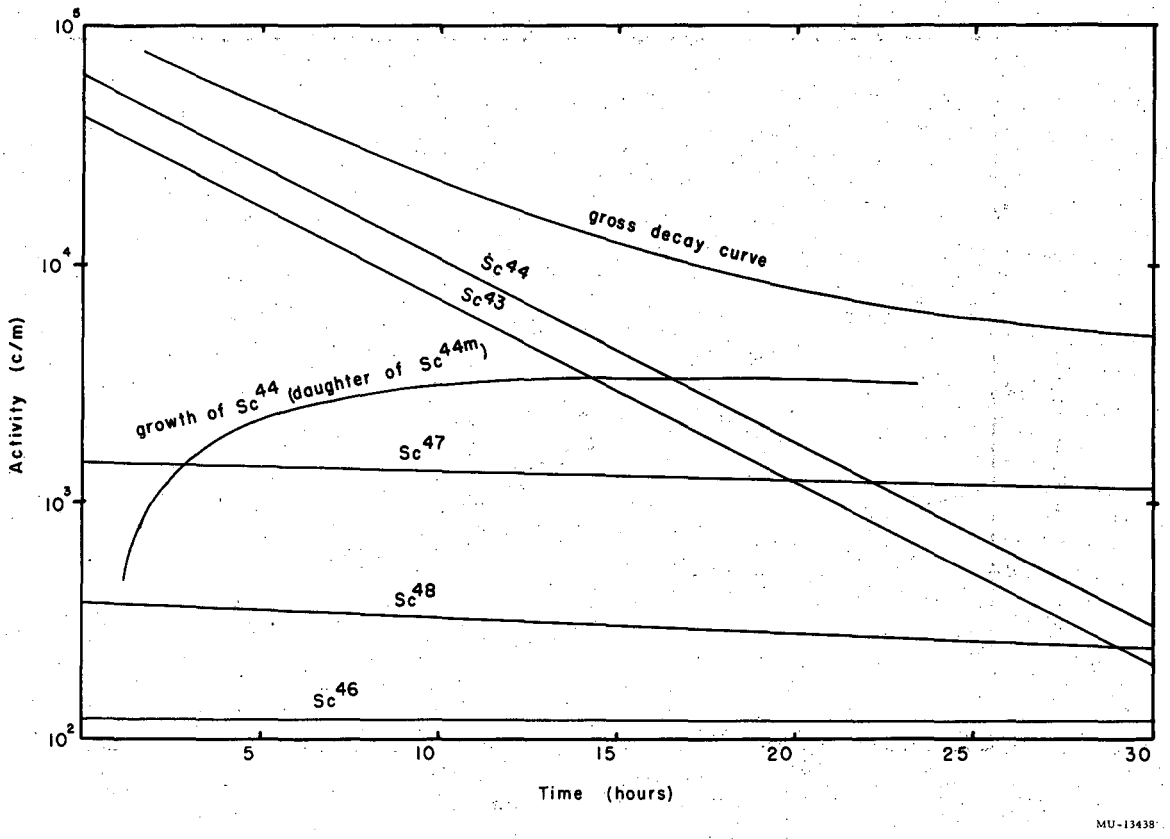

Fig. 5(b). Proportional-counter decay-curve resolution of short-lived scandium isotopes.

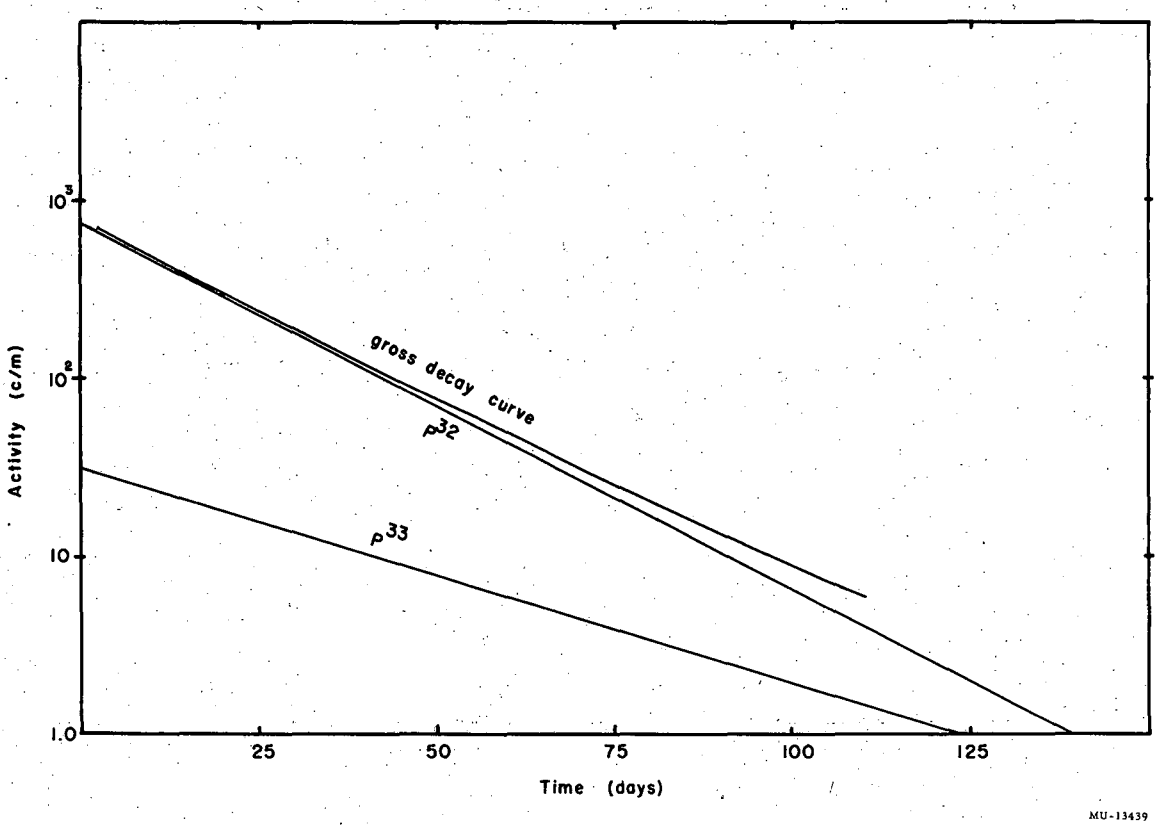

Fig. 6. Least-squares resolution of the proportional-counter decay curve of a phosphorus sample obtained in this work.

3. Synthetic Plots

Although the least-squares method was used in this study wherever necessary for decay-curve analysis, mention will be made of two other graphical methods, which were tested and found acceptable for use in resolving the type of problem described in the previous section. One of these is the synthetic plot, in which the two components to be resolved from a decay curve are drawn with respective half-lives on semi-log paper with an arbitrary activity scale. The two lines are then added over a fairly large time interval to give an over-all decay curve some portion of which the actual data will fit. The resolved lines can then be traced onto the true decay curve. The method is applicable to parent-daughter resolution also.[3]

4. Biller Plot

The basis for this method of resolution may be seen by writing the equation for the total activity in a two-component system,

$$A = A_1^o \; e^{-\lambda_1 t} + A_2^o \, e^{-\lambda_2 t}, \qquad (2)$$

where A = total activity measured at time t,

A_x^o = activity of component x at end of bombardment,

λ_x = decay constant of component x.

Multiplying both sides by $e^{+\lambda_1 t}$, one obtains

$$A \, e^{+\lambda_1 t} = A_2^o \, e^{(\lambda_1 - \lambda_2)t} + A_1^o, \qquad (3)$$

which has the form $y = m\,x + b$, a straight line whose slope is equal to the activity of Component Two at end of bombardment, and whose y intercept at $x = 0$ is the activity of Component One at this time. Both the synthetic and Biller-plot methods are limited in accuracy because of their graphical nature, but they may aid in resolving a part or parts of a complex decay curve.

B. Determination of Disintegration Rates

1. Conversion of Beta-Particle Counting Rates to Disintegration Rates

For the calculation of cross sections, the counting rates at end of bombardment obtained by one of the methods of decay-curve analysis must be converted to disintegration rates, which is the true

measure of the yield of an isotope formed in a bombardment. The corrections that must be applied in the case of beta-particle counting have been studied by several investigators.[32,33] The counting rate of a sample may be written as the product of several factors,

$$A^{\circ} = D^{\circ} G f_W f_C f_A f_H f_E f_S f_B f_D, \qquad (4)$$

where A° is the activity of a beta-emitting nuclide corrected for background rate,

D° is the disintegration rate of the nuclide,

G is the geometry factor, defined as the fractional solid angle at the sample subtended by the counter window,

f_W is the factor for the effect of the beta-particle absorption by the counter-tube window and the air in the space between the tube and the source,

f_C is the factor for the effect of the finite resolving time of the counting tube and circuit,

f_A is the factor for the effect of air in scattering beta particles into the counter (separated for convenience from the effect due to air absorption),

f_H is the factor for the effect of the source-support structure and walls of the housing in scattering beta particles into the counter,

f_E is the factor for the efficiency of the counter; it is defined as the ratio between the number of particles counted and the number of particles that penetrate the counter window,

f_S is the factor for the effect of the mass of the source in causing both scattering and absorption of beta particles,

f_B is the factor for the increase in counting rate due to backscattering by the material supporting the source,

f_D is the decay-scheme correction.

The following is a brief discussion of each of these corrections and the assumptions made in this work concerning them.

(a) Coincidence correction, f_C:

The chlorine-quenched Geiger counters that were used for a small portion of this work had a coincidence correction of 0.45% per 1000 counts per minute as determined by the method of split sources.

The methane-flow proportional counters had no detectable coincidence correction up through 10^5 counts per minute, so that it is probably 1/50 or 1/100 of the Geiger-counter figure, and it was neglected on these counters.

(b) Air and housing scattering, f_A and f_H:

These effects have been shown to be small[32] for an aluminum-lined lead housing such as the ones used in this work, and they were neglected.

(c) Efficiency of the counting tubes, f_E:

This factor was assumed to be unity for both positrons and negatrons. An experiment using soft Co^{60} and hard Na^{24} negatrons indicated that there was no energy dependence in this factor.

(d) Air-window absorption, f_W:

For the spectrum of beta particles emitted by a radioactive sample, absorption is exponential for small absorber thicknesses. This fact enables one to determine an empirical formula, relating an absorption coefficient μ and maximum beta energy E_{max}, from which f_W can be calculated by the relation

$$f_W = \exp(-\mu t), \tag{5}$$

where μ is the absorption coefficient,

t is the thickness of air plus window, in mg/cm^2.

The following empirical relation given by Gleason, Taylor, and Tabern[34] was used for obtaining the absorption coefficients:

$$\mu = 0.017\ E_{max}^{-1.43}. \tag{6}$$

These relations were checked, using hard and soft beta emitters by actual measurements with thin aluminum absorbers, and found to hold within experimental error. Consequently, the factors f_W were usually calculated for nuclides by means of these equations.

(e) Backscattering correction, f_B:

The effect of an increase in the counting rate due to the backscattering of beta particles from the sample mount is a function of the beta energy and the backing material, and to a small extent depends on the geometry of the counting arrangement,[35] although it was assumed constant at all geometries in this work. Because aluminum cards were used for mounting samples in this work, the saturation

backscattering factors for this element were taken from the data of Burtt.[33] In addition, this effect is smaller for positrons than for negatrons, as pointed out and explained by Seliger.[36] As a result, all positron counting rates were increased by 10% to make them comparable to negatron rates.

(f) Self-scattering and self-absorption correction, f_S:

This correction is a function of the beta energy and the thickness of the sample. For thin samples, self-scattering is predominant, and this results in an increase in the counting rate. As the sample thickness increases, the effect approaches exponential absorption of beta particles in a material of known density, and the counting rate is accordingly decreased. In this study, the self-scattering, self-absorption factors determined by Nervik and Stevenson[37] were used exclusively. There is no evidence that the factor is strongly affected by the geometry, therefore it was assumed to be constant on all shelves.

(g) Geometry factor, G:

Only a portion of the activity emanating from a sample reaches the counting chamber and is recorded. This fraction is determined by the geometry of the counting arrangement, which may be measured experimentally for each shelf. For this study, it actually was not necessary to determine the geometry factors for the counters used, since disintegration rates were eventually compared with the Na^{24} monitor, which could be counted under the same geometry conditions as the samples in every bombardment. However, for other types of experiments and for general laboratory use, these factors were measured for the Berkeley proportional counters by the following three methods:

1. BUREAU OF STANDARDS Ra DEF No. 3216. This standard was counted through 3.8 mg/cm^2 of aluminum placed next to the window to minimize scattering effects. The absorber was necessary to cut out alpha particles. The half-life was taken to be 22.2 years. The backscattering factor from the palladium mount was assumed to be 1.61 and the self-scattering, self-absorption correction 1.08. Air-window absorption corrections were measured by taking an aluminum absorption curve on each shelf.

2. SODIUM-24. All counters were calibrated for beta-counting of Na^{24} in 3-mil aluminum foils by determining the disintegration rate in a hot sample prepared with an (n,α) reaction on aluminum in the 60-inch cyclotron, using a beta-gamma coincidence counting technique.[38] Tabulations of all the proportional-counter shelf factors determined in this experiment are available in the UCRL Chemistry Department reference file. The actual shelf geometries may be obtained from these data if a backscattering factor of 1.27 for the aluminum mount and a self-scattering, self-absorption correction of 1.13 for this size foil are used with an absorption-curve determination of the air-window corrections.

3. COBALT-60. A weightless sample of Co^{60} was prepared from a tracer solution and the beta-gamma coincidence counting technique used to determine the disintegration rate in this sample. Geometries were calculated assuming a self-scattering, self-absorption factor of unity and a backscattering factor of 1.19 for the aluminum mount. Air-window corrections were obtained through an aluminum absorption curve on each shelf.

For Shelf Four of a typical counter, the following results were obtained for the geometry factor for these three samples:

Ra DEF	SODIUM-24	COBALT-60
10.6%	11.2%	11.2%

(h) Decay-scheme correction, f_D:

In negatron-emitting isotopes, decay takes place 100% by beta-minus emission, that is, f_D equals unity. A knowledge of the percentages of different beta groups is necessary when they exist in the decay of a nuclide in order to weight the backscattering and self-absorption corrections accordingly, although the errors made are not large if these percentages are known only approximately. Positron emitters, on the other hand, may decay alternately by the electron-capture process, the radiations from which are not efficiently detected by window proportional counters of the type used in this work. It is therefore necessary to know the branching ratio between positron emission and electron capture, and in these cases, the factor f_D is the fraction of the total decay taking place by the emission of positrons. The information for making decay-scheme corrections was taken from the recent compilations by Way,[39] Ajzenberg and Lauritsen,[40] and Endt and Kluyver[41] and stated in Section IV.

All beta-counting rates were corrected for small gamma-ray contributions, which were determined by counting the samples through thick absorbers. For the isotopes studied, internal conversion of gamma rays is quite small, so that the conversion-electron contribution to beta-counting rates was neglected.

2. Conversion of Gamma-Ray Counting Rates to Disintegration Rates

Depending on their energy, gamma rays interact with matter by one of three processes: photoelectric process; Compton scatterings; pair production. The first of these leads to a discrete energy deposition, which appears in a sodium iodide crystal as light whose intensity is proportional to the energy of the gamma ray. This is utilized in the conventional scintillation spectrometer to display a spectrum of photopeaks associated with gamma rays of various energies striking the crystal. These photopeaks have a nearly Gaussian shape, and the area under one of them represents the counting rate of that particular gamma ray. An example of a simple spectrum containing a single gamma ray is shown in Fig. 7.

There are fewer corrections that must be applied to gamma-ray counting rates than for beta particles in order to obtain the disintegration rate of a nuclide. They are the counting efficiency, the geometry, and the decay-scheme correction, and the following is a short discussion of each of these factors with the assumptions made in this work concerning them.

(a) Counting efficiency:

Since the probability of a gamma ray's undergoing a photoelectric event decreases with increasing energy of the photon, the sodium iodide photopeak efficiency decreases accordingly. For the size of crystal used in this work, these efficiencies have been determined by Kalkstein and Hollander[42] as a function of photon energy up to 1.5 Mev and for several sample-to-crystal distances. Their data were used throughout this work.

(b) Geometry factor:

The shelf geometries for the scintillation spectrometer were determined by two methods.

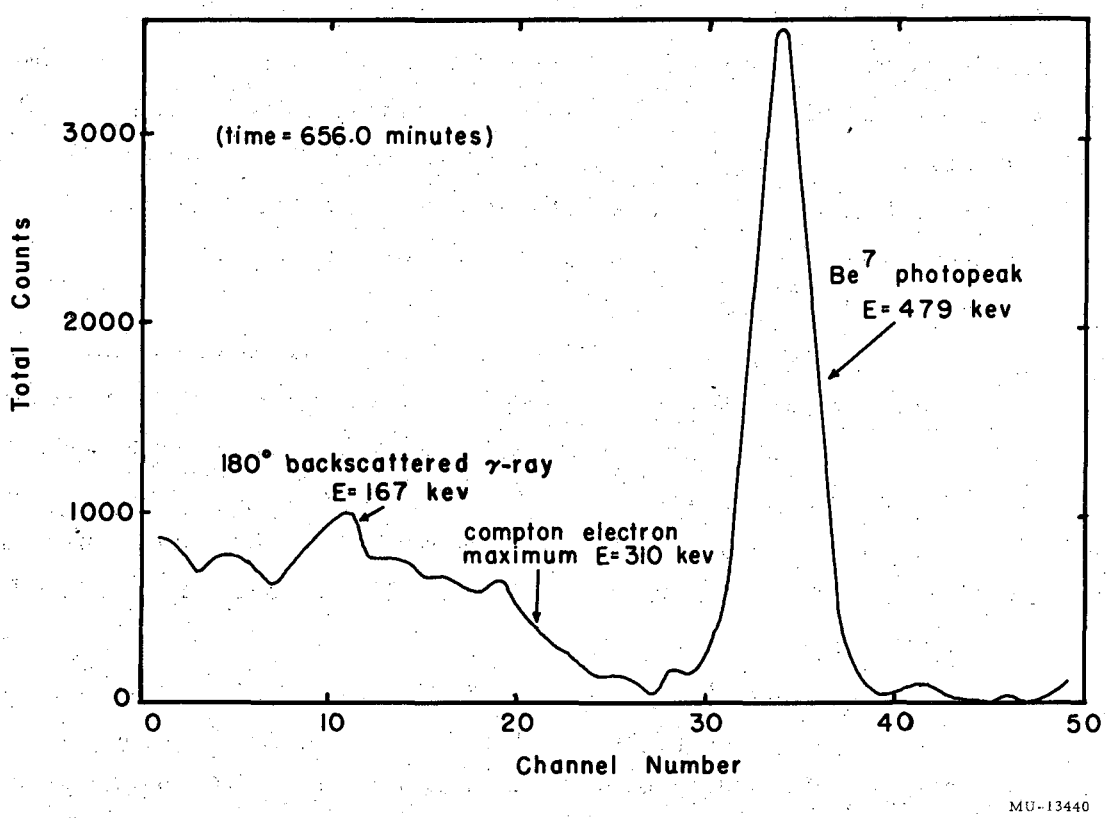

Fig. 7. Gamma-ray spectra of a sample of Be^7 obtained from a Bevatron bombardment.

1. AMERICIUM-241. The 60-kev gamma ray that occurs in the decay of this isotope was used for geometry determinations. The method has the advantage that the counting efficiency of this low-energy photon is unity on all shelves. The gamma-to-alpha ratio was taken to be 0.370.[43]

2. SODIUM-24. A check on the above figures was made by using the Na^{24} sample whose absolute disintegration rate had been determined in the beta-gamma coincidence experiment. In this case, the photo-peak associated with the 1.37-Mev gamma ray, which occurs in 100% of the decays in this isotope, was used in conjunction with the counting efficiencies from the above reference to calculate the geometries. Agreement to within 2% was obtained between these two methods.

(c) Decay-scheme correction:

A knowledge of the fraction of the total decays that take place through the particular gamma ray being observed is necessary to determine the disintegration rate. These abundances were taken from the compilations by Way,[39] Ajzenberg and Lauritsen,[40] and Endt and Kluyver[41] and explicitly stated in Section IV. Internal-conversion coefficients were negligibly small for all the gamma rays looked at in this work.

In addition to the above corrections, there are others that sometimes have to be applied to the observed counting rate in order to arrive at the true photopeak activity. They are as follows:

(d) Escape-peak loss:

In some of the photoelectric events that occur, iodine K x-rays may escape from the edge of the crystal, giving rise to a photo-peak whose energy is that of the principal peak minus the energy of iodine K x-rays, which is about 29 kev. These are photoevents under-gone by the gamma ray, however, so that this escape-peak counting rate must be included in the photopeak integration. The fraction of the activity appearing in the escape peak is a function of the photon energy and the geometry of the counting arrangement, and has been studied by Axel.[44] As the energy of the gamma ray increases, the escape peak is amalgamated into the main photopeak in spectrometers of normal resolution, and the effect is no longer observed.

(e) Absorption:

In the counting of very low-energy gamma rays, absorption in the beryllium window and magnesium oxide reflector may be significant enough to warrant correction. In addition, it is advisable to count samples that are emitting beta radiation in addition to the gamma quanta through a beryllium absorber thick enough to absorb the beta rays, since they contribute a broad distribution of pulse heights if allowed to hit the crystal. The small amount of gamma-ray absorption that occurs in these absorbers may be corrected for using the absorption coefficients of Davisson and Evans.[45] It should also be pointed out that in the counting of annihilation radiation, it is essential that the sample be tightly sandwiched by sufficient absorber to stop all positrons, so that the geometry of the annihilations is defined as accurately as possible. This was done in this work by placing aluminum disks on top of the samples mounted on the thick aluminum cards.

(f) Coincidence or stack-up correction:

When an isotope has coincident gamma rays in its decay, a photopeak may be observed corresponding to the sum of the energies of the separate gammas in a certain fraction of the events. These again are photoelectric events undergone by the gamma rays, and the stack-up peak counting rate should be added to each of the photopeak integrations of the individual gammas giving rise to this stack-up. However, it is better to count the sample at a lower geometry, which tends to eliminate this effect.

3. Conversion of X-Ray Counting Rates to Disintegration Rates

In the conversion of x-ray counting rates to disintegration rates, corrections must be made for the geometry-efficiency of the counting arrangement, absorption in the sample, fluorescent yield, and the decay-scheme branching. The following discussion concerns the assumptions made in this work for these effects.

(a) Absorption in the sample:

The x-rays observed in this study were of such low energies that their absorption in the sample must be corrected for. X-ray absorption is exponential, and the correction factor f_s was determined by averaging the absorption over the sample in the following manner:

$$f_s = \frac{\int_0^t e^{-\mu t}\, dt}{\int_0^t dt} = \frac{1 - e^{-\mu t}}{\mu t} . \qquad (7)$$

Separate factors were calculated for the fraction of the total sample thickness corresponding to the different chemical compositions of the samples, since the mass-absorption coefficients for x-rays, which were taken from the data of Allen,[46] are quite strongly dependent on the atomic number of the absorbing material. The over-all absorption correction is the product of the separate contributions.

(b) Fluorescent yield:

For a given electron shell, the fluorescence yield is defined as the ratio of the number of x-rays actually emitted to the total vacancies available. Since K-electron capture is predominant in the region of this study, the fluorescent yields were taken from the data of Burhop[47] and Broyles.[48]

(c) Decay-scheme correction:

As in beta and gamma counting, it is necessary to know the fraction of the total decays taking place by the electron-capture mode of decay. These data were taken from Way.[39]

(d) Geometry-efficiency factor:

A geometry-efficiency factor for the x-ray counter was determined for the titanium x-rays in the decay of V^{48} and V^{49} by following the decay of the x-ray peak and also making a separate determination of the disintegration rate of V^{48} by both beta and gamma counting. An application of the corrections (a) through (c) above to that part of the x-ray counting rate due to V^{48} then permitted a geometry-efficiency factor to be calculated. The data of Studier and James[49] on the variation of x-ray counting efficiency in argon gas as a function of the photon energy was used to determine this geometry-efficiency factor for counting the manganese K x-rays in the decay of Fe^{55}.

C. Cross-Section Calculations

The following differential equation expresses the rate of change of the number of radioactive atoms of an isotope during a bombardment and serves also to define the cross section,

$$\frac{dN_x}{dt} = I\, n_T\, \sigma_x - \lambda_x N_x, \tag{8}$$

where I is the number of protons hitting the target per unit time,

n_T is the number of target nuclei per square centimeter,

σ_x is the cross section of isotope x in square centimeters,

λ_x is the decay constant of isotope x,

N_x is the number of atoms of isotope x.

If the beam current I is considered constant, and if the condition is imposed that N_x equals zero when t equals zero, this linear first-order equation has the solution

$$\sigma_x = \frac{N_x \lambda_x}{I\, n_T\, (1 - e^{-\lambda_x t})}. \tag{9}$$

Since, in this study, all cross sections were compared with that for Na^{24} production in aluminum, the ratio may be written as follows, where "y" represents Na^{24}:

$$\frac{\sigma_x}{\sigma_y} = \frac{I\, N_x \lambda_x\, n_{Al}\, (1 - e^{-\lambda_y t})}{I\, N_y \lambda_y\, n_T\, (1 - e^{-\lambda_x t})}. \tag{10}$$

The actual beam intensity cancels out in this ratio. Also, since in this study the copper and aluminum foils were matched in area, n is given by

$$n = \frac{W}{M}\ 6.02 \times 10^{23}, \tag{11}$$

where W is weight of foil in grams,

M is molecular weight of foil material.

With this substitution, the cross section for nuclide x formed in the bombardment of copper becomes

$$\sigma_x = \sigma_y \frac{M_{Cu}\, DPM^{o}_{x}\, W_{Al}\, (1 - e^{-\lambda_y t})}{M_{Al}\, DPM^{o}_{y}\, W_{Cu}\, (1 - e^{-\lambda_x t})}, \tag{12}$$

where DPM^{o} represents the disintegration rate at end of bombardment of nuclide x or Na^{24} and is equal to $N^{o}\lambda$. For long-lived nuclides in which there is essentially no decay during bombardment, the factor $(1 - e^{-\lambda_x t})$

may be replaced by the first term in the series expansion of this expression:

$$(1 - e^{-\lambda_x t}) \cong \lambda_x t. \qquad (13)$$

A cross-section expression for the stop-and-start type of run sometimes experienced on the Bevatron in the early phases of this work is given by Shudde.[3]

IV. EXPERIMENTAL RESULTS

A. Nuclides Observed

TRITIUM:

The only activity observed in the hydrogen fraction was 12.26-year tritium. The sample of tritium contained about 1000 counts per minute on the proportional counter and showed no decay at all during counting over a 6-month period, making the assignment of this activity to tritium quite certain. The cross-section calculation involved applying a 32% correction for the recoil loss of tritons out of the copper foil, which was only 212 mg/cm^2 thick. This figure was arrived at on the assumption that the tritons formed are mainly evaporation products with a mean energy of 12 Mev. The range of tritium in copper was taken as 140 mg/cm^2.[17] Calcium was used as an internal monitor in this case to eliminate the possibility of any triton contribution from aluminum.

BERYLLIUM:

The beryllium samples contained no beta activity, attesting to their chemical purity. Gamma-ray spectra showed only the 479-kev photopeak associated with Be^7, the abundance of which was taken to be 12%. The best sample obtained had 32 counts per minute in the photopeak, which decayed with a 53-day half-life.

CARBON:

The only sample of carbon activity obtained was in a run designed to look at argon isotopes. The 20.5-minute C^{11} appeared in the argon fraction as an impurity, but its assignment was unambiguous after subtraction of the activities of A^{37} and A^{41} from the over-all decay curve.

It was assumed that the carbon activity mixed completely with the argon carrier gas, and the same chemical yield for carbon as for argon was used in the cross-section calculation. Consequently this figure is listed as a lower limit.

FLUORINE:

The only activity observed in the fluorine samples was 1.87-hour F^{18}. The samples were counted in proportional counters, and decay was assumed to take place 100% by positron emission.

SODIUM:

The sodium samples always showed the 15.0-hour beta activity of Na^{24}, and the sample from one long bombardment tailed into 13 proportional counts per minute of a long-lived activity which decayed only slightly when followed over a 6-month period. The assignment of this activity to 2.60-year Na^{22} is quite certain, and it was assumed to decay 90% by positron emission. Gamma spectra of Na^{24} samples showed the 1.37-Mev photopeak, which agreed with proportional counting on the disintegration rate if the abundance of this gamma ray is taken to be 100%.

MAGNESIUM:

The only activity seen in magnesium samples was 21.3-hour Mg^{28}, the negatrons of which were counted in equilibrium with those from the Al^{28} daughter on a proportional counter.

SILICON:

The only silicon activity observed was that of 2.62-hour Si^{31}, which decays completely by negatron emission. It was counted in a proportional counter.

PHOSPHORUS:

It was necessary to employ a least-squares analysis to resolve 14.4-day P^{32} and 24.8-day P^{33} in samples of this element, but both these negatron-emitting isotopes were observed. Counting was done in a proportional counter.

SULFUR:

The only sulfur sample obtained was removed from a foil that had been allowed to cool for two weeks after having been bombarded. As a result, there was no chance of seeing the new isotope, S^{38}, discovered recently by Nethaway and Caretto,[50] who tentatively report a half-life of about 170 minutes for it. However, the sample did contain 87.1-day S^{35}, decaying completely by the emission of negatrons, which were counted in a proportional counter.

CHLORINE:

The activities of Cl^{34m}, Cl^{38}, and Cl^{39} were identified in the chlorine fractions. The 33.0-minute Cl^{34m} was studied through the 510-kev photopeak due to the annihilation of the positrons emitted in 100% of the decays of this nuclide. Since these positrons have very high energy, it was necessary to sandwich the samples between a pair of 2-g/cm^2 copper absorbers in order to define the geometry of the annihilations. Chlorine-39 was studied through a lower-energy gamma ray, determined in this work to be 246 kev, which agrees with the most recent data on the decay scheme of this isotope.[51] Its abundance was taken to be 45%, and the half-life 55.5 minutes. The known disintegration rates of these two chlorine isotopes were then converted to beta-particle counting rates and subtracted from the total proportional counter activity observed, and in this way, the activity of 37.3-minute Cl^{38} in the samples was determined. It decays by negatron emission.

ARGON:

Argon-37 and A^{41} were easily resolved from the proportional-counter decay curve of this sample. The former is a 35-day isotope decaying by K and L electron capture, the radiations of which are efficiently counted in the gas-counting setup used. Argon-41 decays by negatron emission with a 1.82-hour half-life.

POTASSIUM:

The proportional-counter decay curves of potassium samples necessitated the use of a least-squares analysis to resolve 12.5-hour K^{42} and 22.2-hour K^{43}. Both isotopes decay by β^- emission.

CALCIUM:

After about two months of counting, proportional-counter decay curves of calcium fractions showed only the 164-day negatron-emitting isotope of Ca^{45}. After subtraction of its activity from the gross curve, a least-squares analysis was done to separate the activities of 4.8-day Ca^{47} and its 3.43-day scandium daughter, which grows in slowly after the last chemical separation of these elements, giving the over-all decay curve a flat initial portion. A check on the disintegration rate of Ca^{47} was obtained by counting the 1.31-Mev gamma ray that occurs in 77% of the decays on the scintillation spectrometer.

SCANDIUM:

All the scandium isotopes were identified by counting selective gamma rays. The isotopes of mass number 43 and 44 have identical 3.92-hour half-lives. They were separated by counting the 510-kev annihilation photopeak, which occurs in 79% of the disintegrations in Sc^{43} and 94% of those in Sc^{44}, and obtaining an independent determination of the disintegration rate of the latter isotope by studying its 1.16-Mev gamma ray also, which is in 100% abundance. The fact that Sc^{44} also grows in from the decay of Sc^{44m} was taken into account and corrected for after the disintegration rate of the isomer was determined by counting its distinctive 270-kev gamma ray, which is 100% abundant. This Sc^{44m} has a 2.44-day half-life. The 3.43-day Sc^{47} was studied through its 160-kev gamma ray in 68% abundance. Scandium-48, which has a 1.83-day half-life, was obtained by looking at its 1.33-Mev gamma ray, occurring in 100% of the decays of this isotope. Finally, 83.9-day Sc^{46} was obtained by means of the 890-kev gamma in 100% abundance after the other gamma rays had decayed out, and its disintegration rate was checked by proportional counting. All disintegration rates were converted to beta-counting rates and added over the whole counting period. The gross proportional-counter decay curve constructed in this manner agreed excellently with that actually observed over several months of counting (see Fig. 5). The limit listed for 57-minute Sc^{49} is on the basis that 10^3 proportional counts per minute could have easily been detected above that present for the other isotopes at the time of the first count.

TITANIUM:

The only activity observed in chemically pure titanium samples was the positron-emitting 3.10-hour Ti^{45}, which was counted on a proportional counter and assumed to decay 84% by positron emission.

VANADIUM:

Vanadium-47 and V^{48} were easily resolved from proportional-counter decay curves of these samples. The former is a 31.0-minute isotope decaying 97% by positron emission. Vanadium-48 decays 57% by positron emission with a 16.0-day half-life. Its disintegration rate was checked by counting the 990-kev and 1.33-Mev gamma rays, which occur in 100% and 98% of the decays respectively. In addition, K x-ray counting gave about 50 counts per minute of 330-day pure electron-capturing V^{49} in one sample. Its cross section was corrected for the parent Cr^{49} contribution.

CHROMIUM:

Chromium-49, a 41.8-minute isotope decaying 92% by positron emission, was resolved easily from a proportional-counter decay curve which eventually tailed into a long-lived activity identified as the V^{48} daughter of 23.5-hour Cr^{48}, which is a pure electron-capture isotope. Chromium-48 itself was studied by means of a pair of gamma rays determined in this work to have energies of 117 and 306 kev and also to be in coincidence. The following decay scheme was formulated:

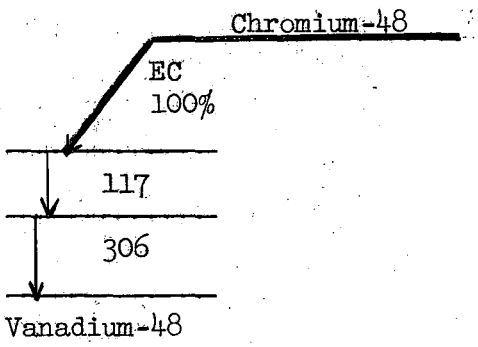

Two groups of workers have since published results in agreement with this scheme.[52,53] The 27.8-day Cr^{51} was also identified in these fractions through its 320-kev gamma ray, assumed to be in 8% abundance. Its cross section was corrected for the Mn^{51} parent contribution.

MANGANESE:

From a proportional-counter decay curve, 5.72-day Mn^{52} and 2.58-hour Mn^{56} could be easily resolved. The first of these decays 33% by positron emission, and a check on the disintegration rate of this isotope was obtained by counting the 730- and 940-kev gamma rays, which are 100% abundant. Manganese-56 is a negatron emitter, and the disintegrations of it were also checked by counting a 100%-abundant 845-kev gamma. When the activities due to these two isotopes had been subtracted from the proportional decay curve, the residual activity was subjected to a least-squares analysis in order to resolve 21.3-minute Mn^{52m} and 45.2-minute Mn^{51}. These are both positron emitters with abundances of 98.5% and 97% respectively. After all these activities had decayed out, gamma-ray spectra of these samples showed the lone 100%-abundant 840-kev gamma associated with the 291-day pure electron-capturing Mn^{54}.

IRON:

The iron isotopes of mass numbers 52, 53, and 59 were easily resolved from proportional-counter decay curves. Iron-53 is an 8.9-minute nuclide decaying 98% by positron emission. Because of its short half-life, experiments involving this isotope were conducted with a stop-watch to record times to the nearest second. Iron-52 is an 8.3-hour isotope decaying 59% by positron emission, and was counted with its 21.3-minute Mn^{52m} daughter in equilibrium. In addition, a check was obtained on the disintegration rate of this nuclide by means of a 163-kev gamma ray discovered in this work and occurring in 100% of the decays of Fe^{52}. The following decay scheme is proposed for the $Fe^{52} - Mn^{52m}$ couple:

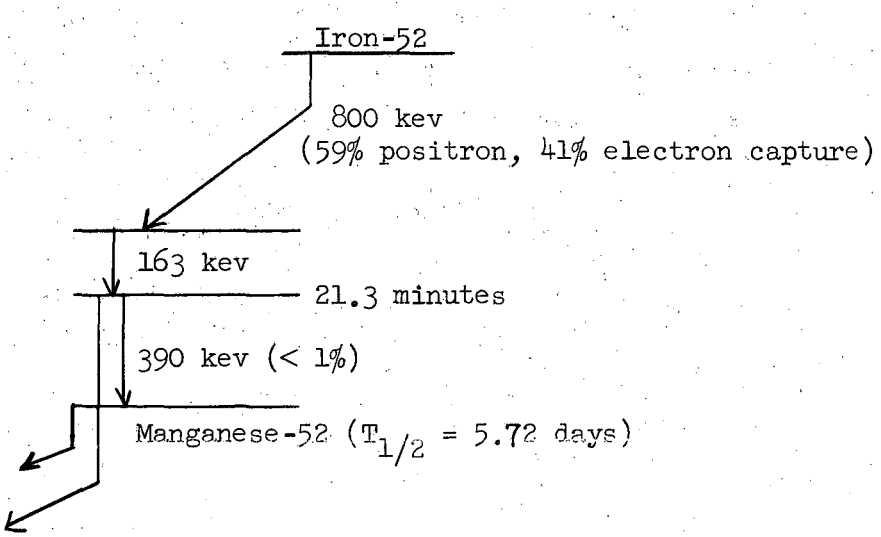

Iron-59 is a 45.0-day β^- emitter. A check in its proportional-counter disintegration rate was obtained by counting the 1.10- and 1.29-Mev gammas occurring with 57% and 43% abundance respectively. Finally, on the x-ray counter, one sample contained about 10 counts per minute of 2.9-year Fe^{55}, which decays entirely by electron capture to the ground state of Mn^{55} (stable).

COBALT:

Proportional-counter decay curves of cobalt samples could be resolved to obtain the activities of 18.0-hour Co^{55}, which decays 69% by positron emission, and the negatron-emitting 1.65-hour Co^{61}. In addition, one sample counted over two years eventually tailed over into 40 counts per minute of 5.25-year Co^{60}. A check on the disintegration rate of the Co^{60} was obtained by counting the 1.17-Mev gamma occurring in 100% of the decays. However, the isotopes of Co^{56}, Co^{57}, and Co^{58} had to be resolved in the scintillation spectrometer for the desired accuracy. Cobalt-56 and Co^{58} have very similar half-lives, which makes their separation difficult. These are 77 days and 71.3 days respectively. The fact that the branching ratio was not known for the former also complicated the counting situation. These isotopes were resolved as follows. The 510-kev photopeak due to positron annihilations was counted. The percentage of the decays of Co^{58} taking place by positron emission was known to be 14.5%. A gamma ray at 840 kev was also counted. It is a composite of 845- and 805-kev gammas in the decays of these two isotopes, the abundances of which were taken to be 82% and 100% in Co^{56} and Co^{58} respectively from the data of Way.[39] In addition, a 1.24-Mev gamma taken to occur in 61% of the disintegrations (see Reference 39) of Co^{56} was counted. With these three pieces of information, the disintegration rates of the two cobalt isotopes could be calculated along with the branching ratio of Co^{56}, which turned out to be

$$\frac{\text{electron capture}}{\text{positron}} = 4.26 .$$

This is equivalent to 19% of the decays taking place by positron emission. A very recent reference[54] quotes the same figure, which also lends support to the disintegration rates determined by the counting procedure described. Cobalt-57 was identified by its clean 123-kev gamma occurring in 100% of

the decays of this 270-day pure electron-capturing isotope. In one sample, an attempt was made to observe the 25-kev gamma ray in the decay of 9-hour Co^{58m} to the Co^{58} ground state. This gamma ray was not seen, but pulse-height analysis is difficult in this energy region. Because of this, no limit is reported for the yield of Co^{58m}.

NICKEL:

Only two activities were observed in nickel fractions. The negatron-emitting 2.56-hour Ni^{65} was easily resolved on proportional-counter decay curves from 36-hour Ni^{57}, which decays exactly 50% by positron emission as determined in this work. In addition, since there was a disagreement concerning gamma-ray abundances in the decay of this isotope, the 128-kev and 1.39-Mev gammas were studied and found to have abundances of 22% and 83% respectively, which agrees with one group of workers who have investigated this nuclide (see Reference 39). The limit placed on the cross section of 6.4-day Ni^{56} is based on a search (results of which were negative) for some of the low-energy gamma rays reported in the decay of this pure electron-capturing isotope. It was assumed that five photopeak counts per minute would have easily been seen.

COPPER:

All the copper activities were resolved from proportional-counter decay curves. The 12.8-hour Cu^{64} emits both β^- and β^+ particles whose sum accounts for 57% of the total decays. Copper-61 is a 3.33-hour isotope decaying 66% by positron emission. After subtraction of these two activities from the gross decay curve, a least-squares analysis was applied to the residual activity in order to resolve the 23.4-minute Cu^{60} and the 9.73-minute Cu^{62}, which decay by 93% and 98% positron emission respectively.

ZINC:

The beta activities associated with 9.33-hour Zn^{62} and 38.3-minute Zn^{63} were easily resolved from proportional-counter decay curves. The former was counted with its 9.7-minute copper daughter in equilibrium with it. Zinc-62 itself decays 26% by positron emission. The percentage of

the decays taking place by positron emission in Zn^{63} was taken to be 90%. In addition, in one long bombardment a zinc fraction was removed and searched for 243.5-day Zn^{65}, which decays entirely by electron capture but has a 1.11-Mev gamma ray in 45.5% of the disintegrations. This long-lived secondary product was observed.

GALLIUM:

Gallium-66 and Ga^{68} were easily resolved from a proportional-counter decay curve of the gallium sample. The half-lives of these secondary products are 9.45 hours and 68 minutes respectively, and they were assumed to decay 60% and 84% by positron emission.

B. Experimental Cross Sections

Table I gives the experimental cross-section results obtained in this work. It is arranged in three columns. The first gives the nuclide; the second gives the cross section in millibarns, which is the weighted average value of the number of separate determinations given parenthetically in the third column. These cross sections are based on a value of 10.5 millibarns for the Al^{27} (p,3pn) Na^{24} cross section discussed in Section II. A realistic figure for the probable uncertainty in these results due to the individual errors in the factors comprising the cross-section calculations and a systematic uncertainty in the monitor cross section is ± 20%.

Table I. Experimental Cross Sections

$T_{1/2}$	Nuclide	E_γ	Cross Section (mb)	Number of Determinations
9.5h	Ga^{66}	1.0,2.8	0.061	(1)
68m	Ga^{68}	1.08	0.064	(1)
9.3h	Zn^{62}	.6	0.20	(2)
38m	Zn^{63}	1	0.87	(2)
245D	Zn^{65}	1.1	0.96	(1)
24m	Cu^{60}	1.3,1.8	3.0	(2)
3.3h	Cu^{61}	.3,.7	15	(5)
9.9m	Cu^{62}	?	32	(2)
12.9h	Cu^{64}	1.34	22	(5)
6.4D	Ni^{56}	~1	< 0.05	(1)
36h	Ni^{57}	1.4,1.9	0.72	(5)
2.56h	Ni^{65}	1.5	0.22*	(3)
18h	Co^{55}	.9,1.4	1.8	(3)
77d	Co^{56}	.9,1.2	5.1	(2)
270d	Co^{57}	.1	24	(3)
71d	Co^{58}	.8,1.6	33	(2)
5.2Y	Co^{60}	1.33	14	(2)
1.6h	Co^{61}	.068	5.3	(2)
8h	Fe^{52}	.17,.4	0.13	(3)
9m	Fe^{53}	.37	1.3	(1)
2.7Y	Fe^{55}	no γ	17	(1)
45d	Fe^{59}	1.1,1.3	0.77	(5)
45m	Mn^{51}	.4	2.2	(2)
20m	Mn^{52m}	.65	1.9	(2)
5.7D	Mn^{52}	1.5	5.2	(6)
314d	Mn^{54}	.8	16	(3)
2.6h	Mn^{56}	.8,2	2.8	(3)
2.3h	Cr^{48}	.3	0.22	(4)
42m	Cr^{49}	.09	2.8	(2)
28D	Cr^{51}	.3	14	(3)
32m	V^{47}	1.5,1.9	3.1	(2)
16D	V^{48}	1,2	10	(3)
330D	V^{49}	no γ	13	(2)
3h	Ti^{45}	?	3.3	(2)
3.9h	Sc^{43}	.37	3.8	(2)
2.4D	Sc^{44m}	.27	4.7	(2)
4h	Sc^{44}	1.2	4.6	(2)
84D	Sc^{46}	1.1	7.8	(2)
3.4D	Sc^{47}	.16	3.0	(2)
44h	Sc^{48}	1.3	0.38	(2)
57m	Sc^{49}	1.8	< 0.5	(1)
165D	Ca^{45}	no γ	1.2	(3)
4.5D	Ca^{47}	1.3	0.086	(4)
12h	K^{42}	1.5	5.4	(2)
22h	K^{43}	.4,1	1.1	(2)
34D	A^{37}	?	5.9	(1)
1.83h	A^{41}	1.3	0.87	(1)
32m	Cl^{34m}	2	0.73	(2)
37m	Cl^{38}	2	2.0	(2)
55m	Cl^{39}	1.3	0.60	(2)
87d	S^{35}	no γ	2.0	(1)
14d	P^{32}	no γ	7.8	(2)
25d	P^{33}	no γ	2.2	(1)
2.6h	Si^{31}	1.3	2.9	(1)
21h	Mg^{28}	.03,1.4	0.65	(2)
2.6Y	Na^{22}	1.3	2.9	(1)
15h	Na^{24}	2.75	4.8	(3)
111m	F^{18}	?	3.4	(2)
20m	C^{11}	no γ	≤3.1	(1)
53d	Be^{7}	.5	16.5	(3)
	H^{3}	no γ	202	(1)

* The cross section for Ni^{65} is based on the isotopic abundance of Cu^{65} rather than natural copper; all the other nuclides are based on the naturally occurring isotopic mixture of copper.

V. DISCUSSION

A. Cross-Section Distributions—Estimation of Unmeasured Yields

An inspection of the experimentally measured cross sections leads to the following general observations:

1. The yields across an isobar, an element, or an isotone are largest in the region of the stable isotopes and fall off rapidly on the wings of these isolines. This is a reflection of the shape of the mass surface that passes through its minimum at the stable isotopes.

2. Many of the measured cross sections are independent in that either they are shielded by stable isotopes from formation through decay, or their yields may be corrected for any contribution from a parent due to decay of the parent. The high cross sections for these products indicate that they are formed directly as a result of proton collisions with copper nuclei. Actually, to a good approximation, all measured yields are independent, owing to the distribution of products and the rapid fall-off of cross sections with distance from the line of stability.

3. Along isodiapheric lines (constant N-Z) originating at the various copper isotopes, the measured cross sections seem to vary in a smooth manner although the respective lines do not necessarily duplicate one another. This is because each line corresponds to a different path along the yield surface, some crossing its valley and others merely wending along its sides. Plots of the cross sections along these lines are shown in Figs. 8 through 15.

These observations lead to the conclusion that the stable isotopes are formed in quite high yield. For estimation of the formation cross sections of stable and unmeasured radioactive isotopes, the previously stated observations were utilized in the following manner. It was assumed that the yields across elements, isobars, and isotones follow a Gaussian distribution, that is, a parabola on a plot of the logarithm of the cross section. Since there are not enough measurable cross sections across any of the isobars below copper to test this assumption rigidly, the method was first applied to the elements cobalt, iron, manganese, and scandium. Three cross sections for isotopes of a given type, namely odd-odd, odd-even, or even-odd, whichever were sufficient to apply the method, were fitted to an equation of the form

$$\log \sigma = a A^2 + b A + c, \qquad (14)$$

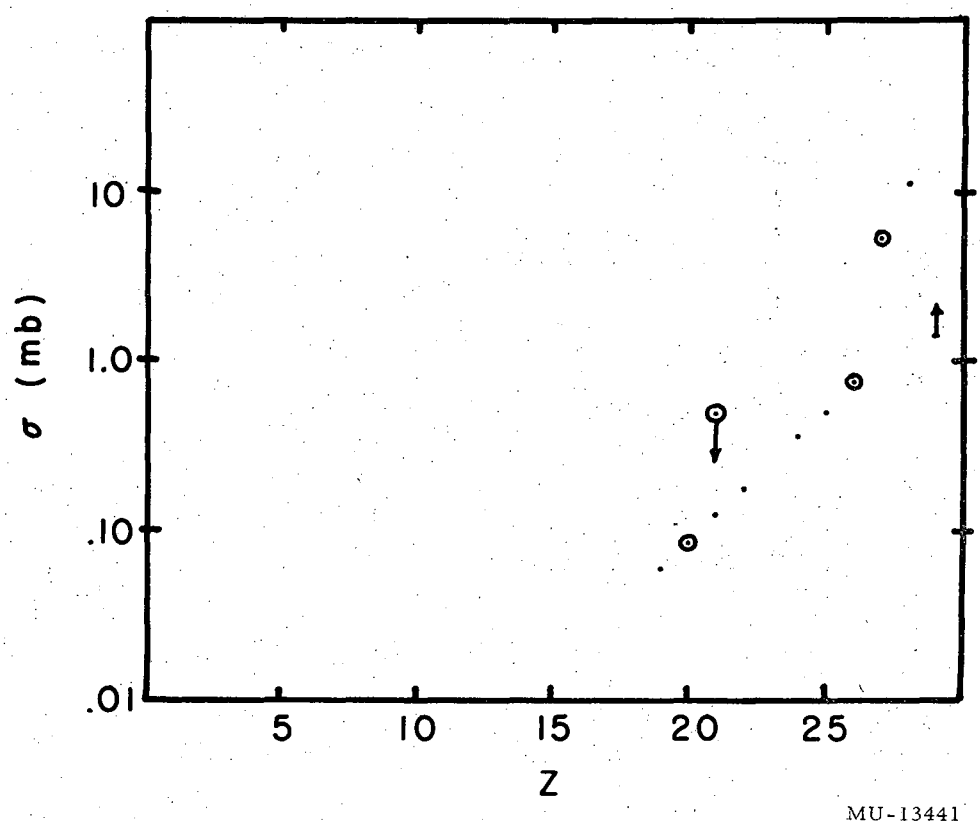

Fig. 8. Isodiapheric series N - Z = 7 (origin at Cu^{65}).

In Figs. 8-15, ⊙ = experimental points; • = interpolations obtained from parabolas across elements.

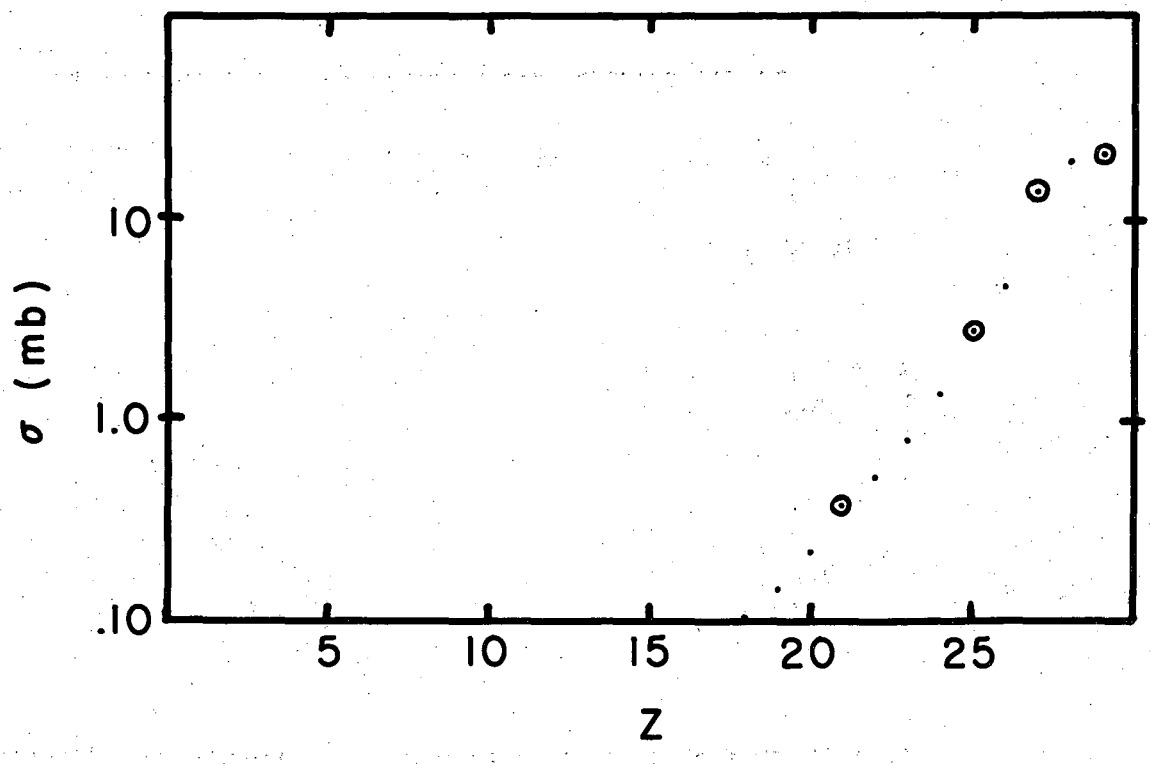

Fig. 9. Isodiapheric series N - Z = 6 (origin at Cu^{64}).

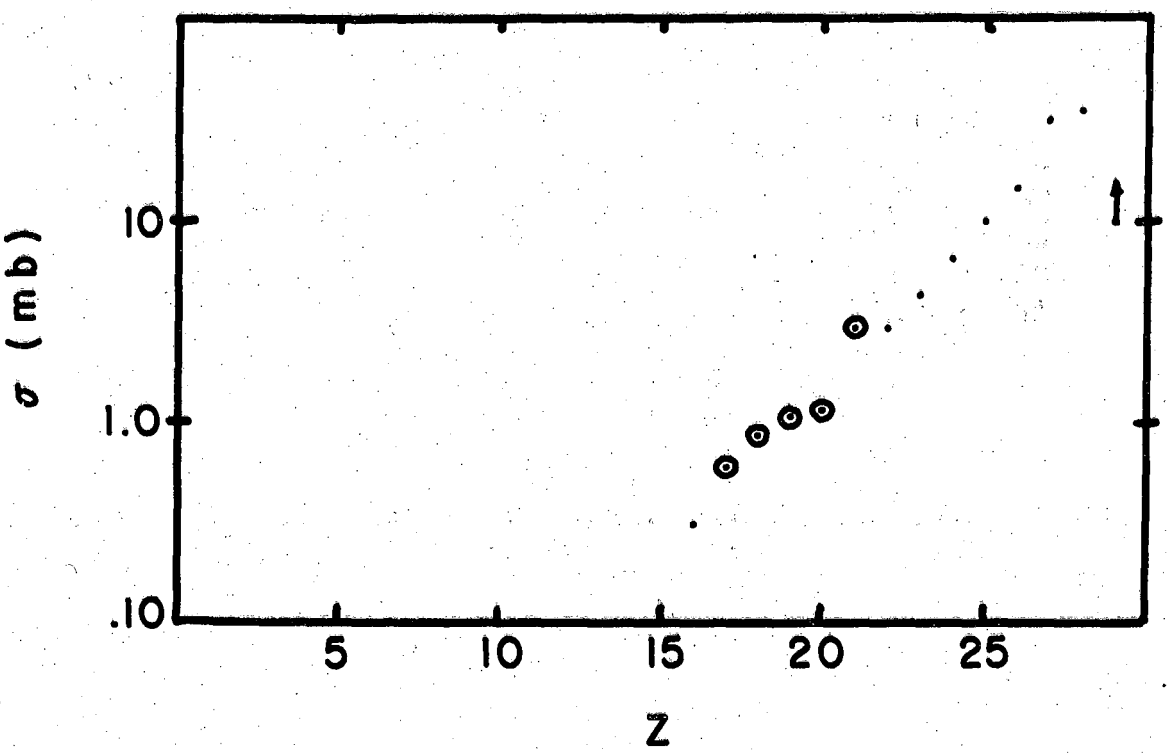

Fig. 10. Isodiapheric series N - Z = 5 (origin at Cu^{63}).

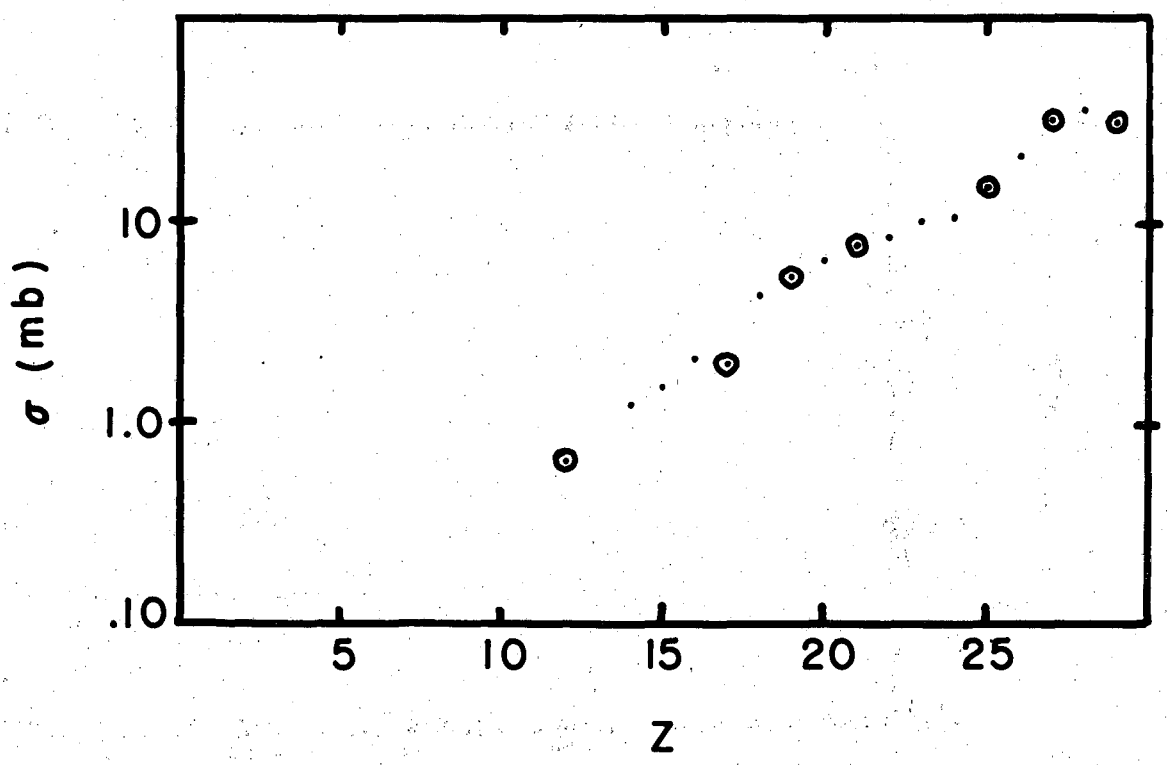

Fig. 11. Isodiapheric series N - Z = 4 (origin at Cu^{62}).

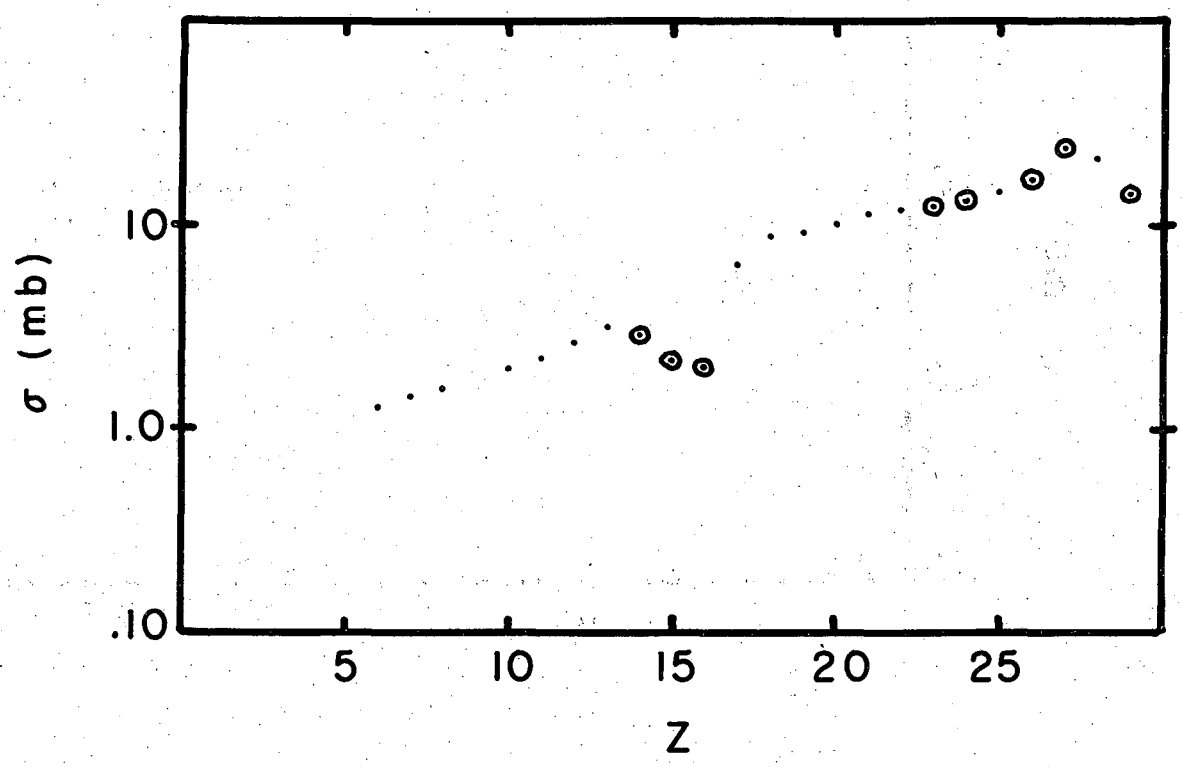

Fig. 12. Isodiapheric series N - Z = 3 (origin at Cu^{61}).

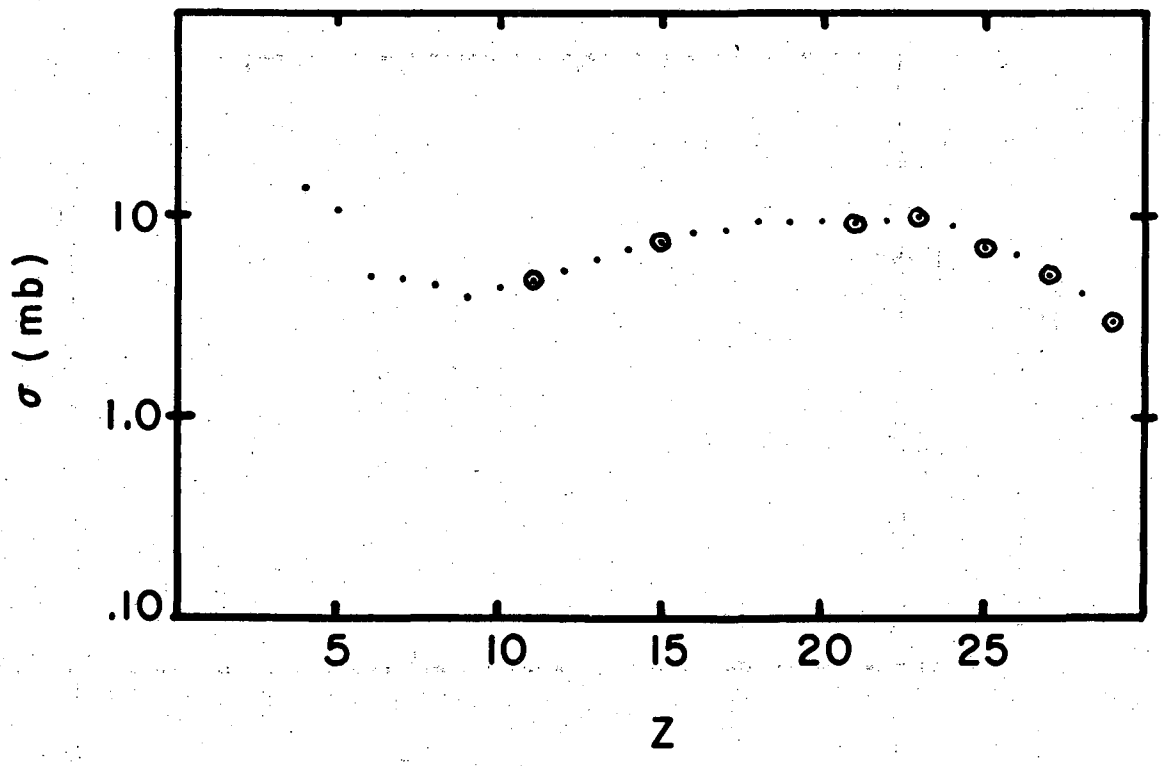

Fig. 13. Isodiapheric series N - Z = 2 (origin at Cu^{60}).

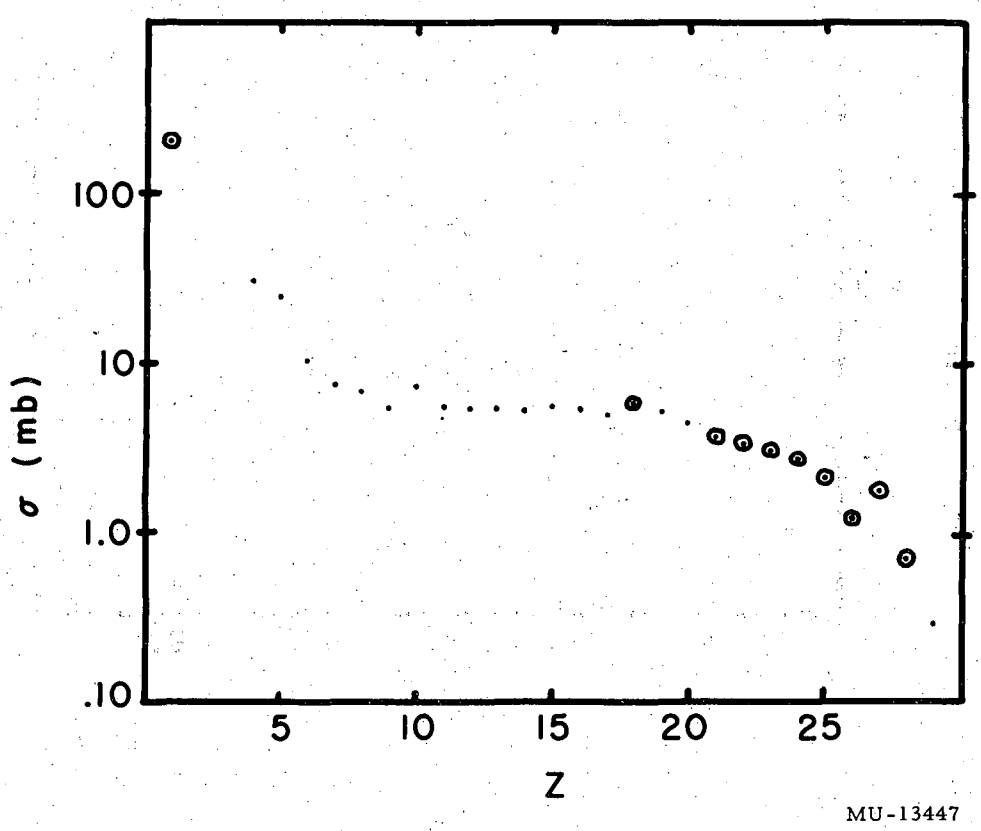

Fig. 14. Isodiapheric series N - Z = 1 (origin at Cu^{59}).

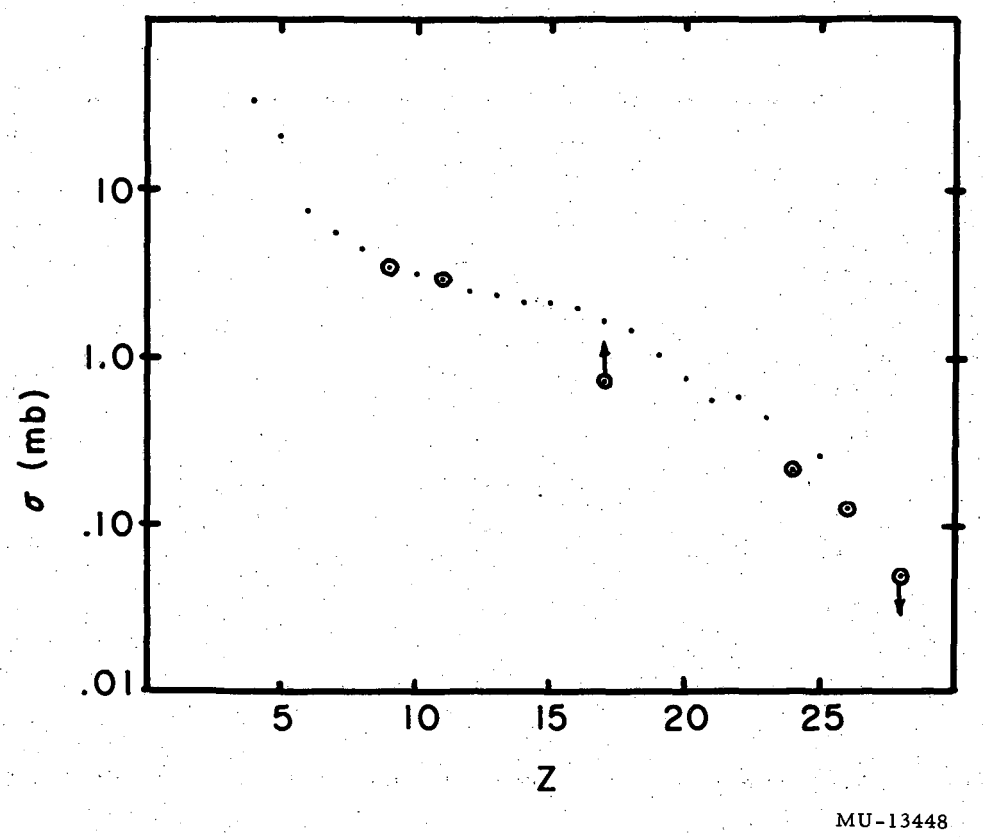

Fig. 15. Isodiapheric series N - Z = 0 (origin at Cu^{58}).

where σ = measured cross section of isotope in millibarns,

A = mass number for that isotope.

Having determined the parameters a, b, and c, one could calculate the cross sections for nuclides of the other type involved and compare them with the actual measured ones. The results are shown in Table II.

These results lead to the following inportant conclusions:

1. Within experimental error, the cross-section distribution across an element does indeed follow the assumed shape.

2. There are no outstanding anomalies in the yields of isotopes of different type as predicted from this distribution, although insofar as this limited portion of the data is concerned, there does seem to be a consistent indication that the yields of odd-even isotopes are of the order of 20% higher than those of odd-odd ones, as seen from the ratio of predicted to measured values. For Co^{56}, the ratio is somewhat higher than the 20% figure quoted, but the cross section for this isotope was very difficult to measure. This conclusion is somewhat surprising in view of the generally accepted assumption that the level density of a nuclide, which governs the final stages of an evaporation process according to the Weisskopf formulation, is greater for odd-odd isotopes than that for odd-even ones, which is in turn greater than that for even-evens, and the cross sections should be favored in this order because of this effect. However, the idea that the separation energies of a neutron or a proton, which also affect the evaporation process, as a rule favor the cross sections in just the inverse order from that above,[55] namely even-even highest, would explain the results if these two effects approximately offset each other. The data are consistent with the latter factor's being slightly favored.

3. The parameter a, which is a measure of the width of the parabola, remained essentially constant for all four elements, indicating that this width is the same at least over this range of atomic numbers (21-28). Its values were

	cobalt	iron	manganese	scandium
a =	-0.121	-0.150	-0.137	-0.154

4. By use of the parameters a and b, the quantity -b/2a was calculated for each of the four elements mentioned. This quantity is the mass number at the peak of the parabola and corresponds to the most probable

Table II. Data for testing the assumption of a parabolic distribution of yields across elements. The type denotes the number of protons and neutrons respectively as being odd or even.

DATA FOR ISOTOPES FITTED TO EQ. (14)				DATA FOR ISOTOPES PREDICTED			COMPARISON	
Element	Mass Number	Type	Cross Section (mb)	Mass Number	Type	Pred. Cross Section	Meas. Cross Section	Ratio: Pred./Meas.
cobalt	55	o-e	1.8	56	o-o	8.7	5.1	1.70
	57	o-e	24	58	o-o	38	33	1.15
	61	o-e	5.3	60	o-o	18	14	1.29
iron	53	e-o	1.3	52	e-e	0.13	0.13	1.00
	55	e-o	17					
	59	e-o	0.77					
manganese	52	o-o	7.1	51	o-e	1.8	2.2	0.82
	54	o-o	16					
	56	o-o	2.8					
scandium	44	o-o	9.3	43	o-e	3.5	3.8	0.92
	46	o-o	7.8	47	o-e	2.4	3.0	0.81
	48	o-o	0.38					

A for a given Z. These were plotted as a function of Z in Fig. 16 and found to be linear. The unmeasured cross sections for all elements between Z = 21 and Z = 28 could then be determined as long as there was one measured cross section for the element, since a parabola of good shape was available from any of the four elements discussed whose maximum in A could be obtained from the above plot. The measured yields for a particular element fixed the vertical scale for its parabola. The above procedure was performed graphically.

The cross sections obtained in this manner were then included in the plots of data along isodiapheric lines shown in Figs. 8 through 15, strengthening the assumption of a smooth variation along these series. In order to ascertain whether or not the above procedure could be extended down to low atomic numbers, the yields for Mg^{24} and Mg^{26} were obtained from isodiapheric-line systematics and used in conjunction with the measured value of Mg^{28} to construct a parabola for this element. Its width parameter, a, was -0.15 as in scandium, and the most probable A for Z = 12 fell nicely on the line previously constructed in Fig. 16. Thus unmeasured cross sections for elements 12 through 21 were determined by the same procedure as described above, using measured cross sections for elements and isodiapheric-line interpolations to keep the whole analysis consistent. Only two experimental results seemed out of line with this treatment of the data. The measured value for S^{35} was lower by about a factor of three than that predicted. This may be due to the possibility that complete exchange between the active atoms and the carrier added was not effected with the chemical separation procedure used. The very soft negatrons emitted in the decay of this isotope also contribute larger-than-average uncertainties in the corrections applied to the counting rate. The only alternative explanation for this deviation would be to assume an effect due to the adjacent 20-neutron closed shell, although one would expect a similar effect for the isotopes adjacent to the 28-neutron shell, which is not observed. Also, the existence of an undiscovered isomer cannot be ruled out. The other exception was the cross section for P^{33}, which was lower by a factor of two than predicted. In this case, the combination of very difficult decay-curve resolution (see Fig. 6) and soft negatrons in the decay could easily account for the discrepancy.

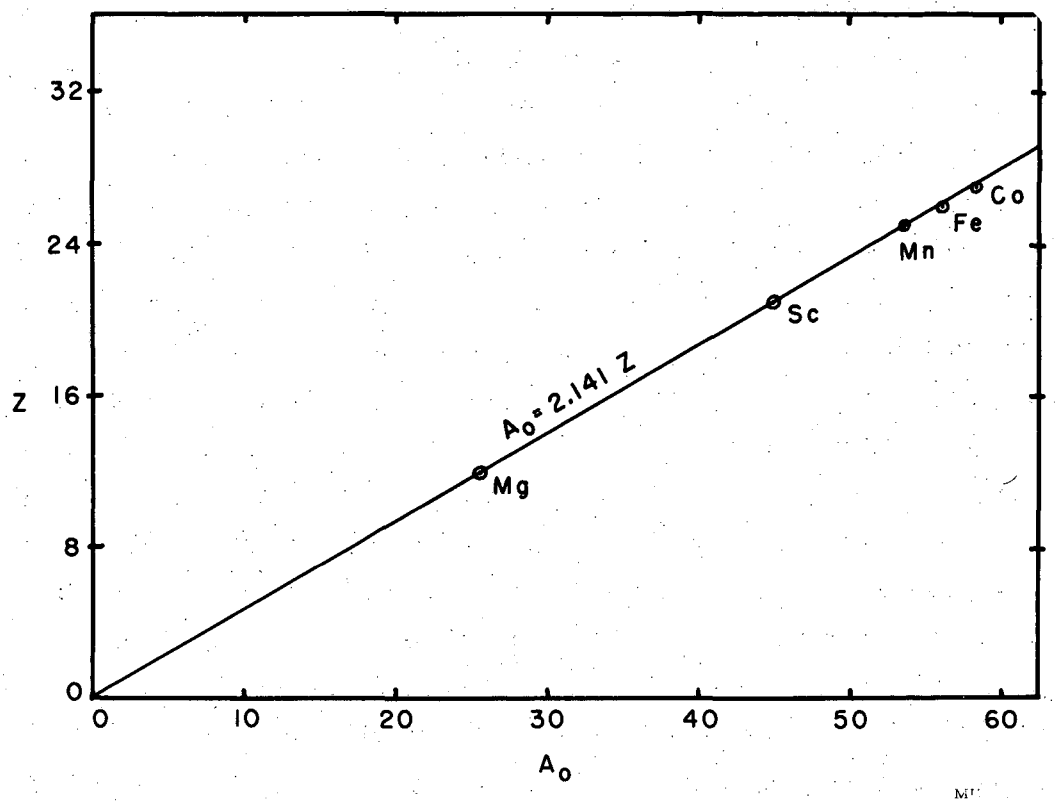

Fig. 16. Most probable mass number A_o for a given atomic number Z.

Since the cross sections for elements below magnesium are of interest to some workers, chiefly because the energy of the protons used in this study represent those of cosmic-ray particles, the interpolation methods described were extended down as far as beryllium, with reservations. In this range of atomic numbers, the sparsity of measured cross sections and the onset of low level densities where individual level structures in nuclides may strongly affect the formation cross sections make the results questionable. In addition, as will be seen presently, the formation of these products is probably due to a different mechanism from that leading to the nuclides already treated, although an understanding of this process indicates that the extension is warrented. Nevertheless, these latter results should be looked upon only with relation to the methods used to obtain them.

Finally, nuclides close to the target, namely those of copper and nickel, were treated individually owing to the presence of the two stable isotopes of natural copper, giving rise to specific effects such as the reactions discussed in Section E. The (p,p') cross section was taken to be > 5 millibarns from the data of Nethaway on In^{115}. [56] The final cross sections for all isotopes, both measured and interpolated, are shown in Fig. 17, which is a "G. E. Chart of the Nuclides" type of plot.

B. Application of a General Cross-Section Formula

To facilitate discussion of the data and to confirm the validity of the parabolic distribution across isobars, three yields for each mass number were fitted to an equation analagous to (14):

$$\log \sigma = a Z^2 + b Z + c, \qquad (15)$$

where Z is now the atomic number of the isotope with cross section σ. Other cross sections in the isobar were then predicted and found to agree with those obtained by the previous methods. The width parameters, a, remained constant, and a plot of the most probable Z for a given A was constructed from the values of -b/2a just as in the previous treatment of elements. It is shown in Fig. 18 with a least-squares straight line passed through the data. The reason for constructing this plot will be made apparent in the ensuing discussion.

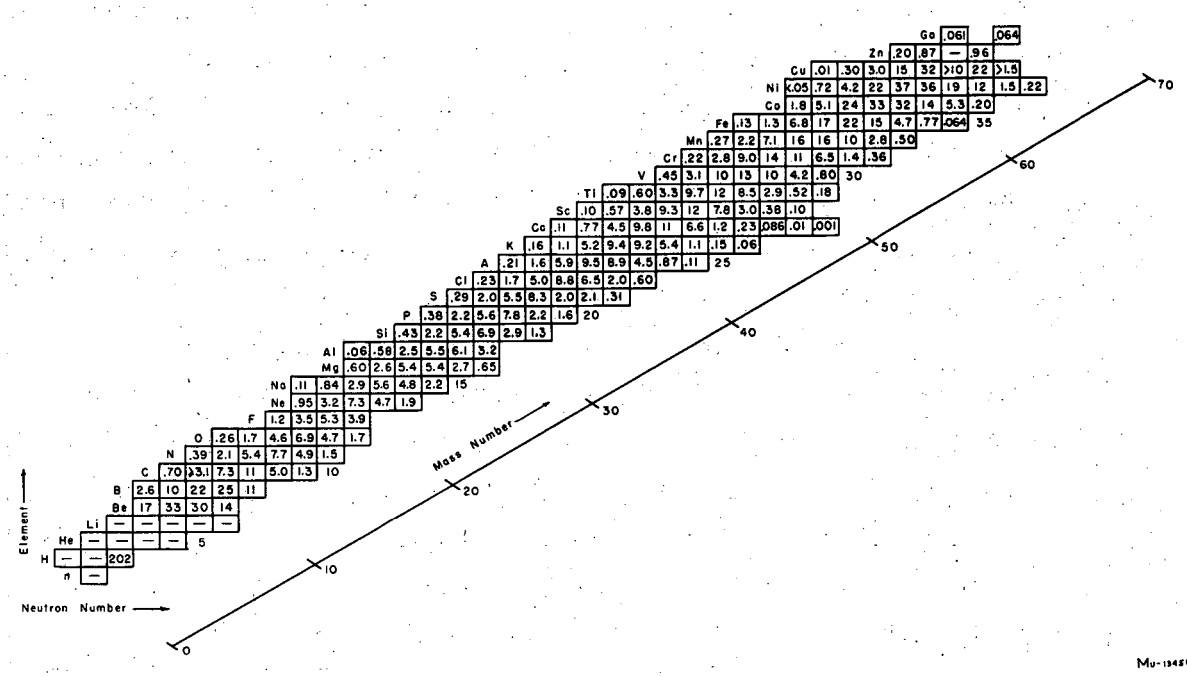

Fig. 17. Summary of measured and interpolated cross sections for all isotopes formed in the 5.7-Bev proton bombardment of copper.

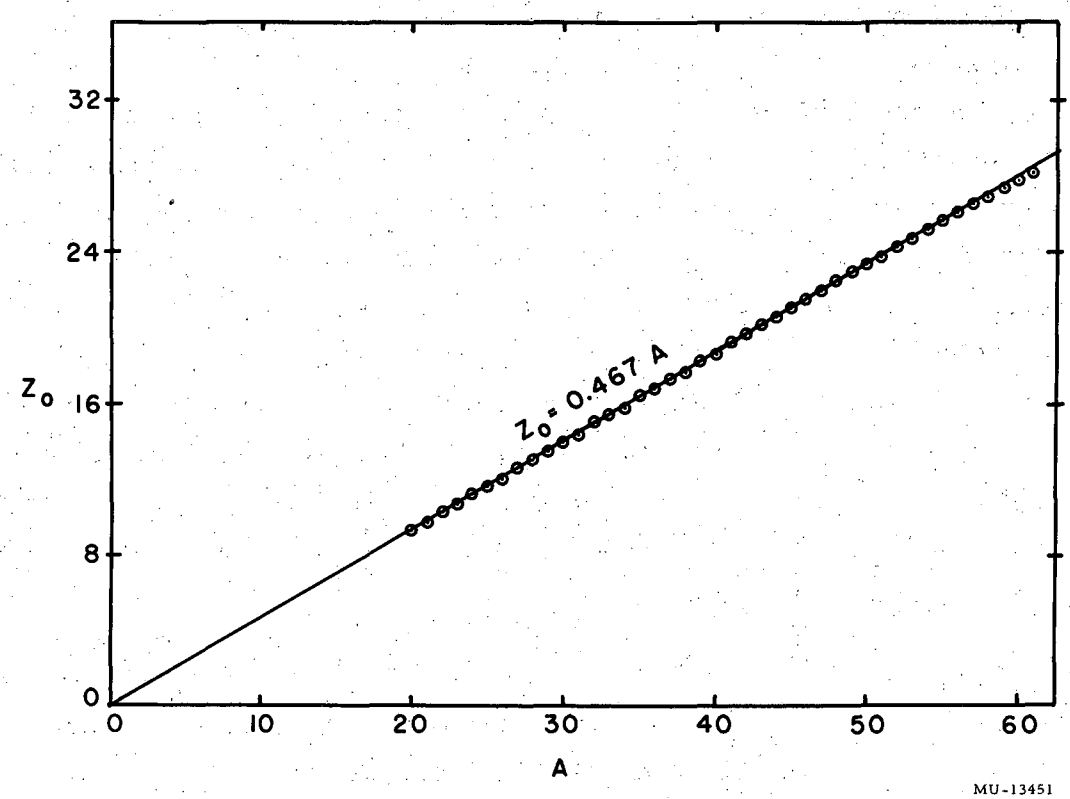

Fig. 18. Most probable atomic number Z_o for a given mass number A.

The cross sections for each mass number were summed and plotted as a function of mass number. The resulting distribution, which is referred to hereafter as the yield-mass curve, is shown in Fig. 19. It is apparent that this over-all curve from A = 61 down to about A = 20 may be approximated by a decreasing exponential expression such as that employed by Rudstam for several spallation studies.[2] Two other observations were made by Rudstam, namely:

1. The independent yield versus the atomic number for isobars is a Gaussian function of the atomic number with a precision index (this quantity is directly related to the width parameter, a, discussed previously) which is independent of the mass number.
2. The most probable Z for a given A can be approximated by a linear function of A passing through the origin.

The detailed study of the data in this work substantiated these assumptions. Consequently, the empirical treatment of the results was carried one step further. The experimentally measured cross sections for 44 of the 59 nuclides studied from mass number 61 to 22 were fitted to the following four-parameter equation,

$$\sigma\,(A,Z) = \exp\,[\,PA - Q - R\,(Z - SA)^2\,], \qquad (16)$$

where $\sigma\,(A,Z)$ = formation cross section for the nuclide with mass number A and atomic number Z.

The parameter S is the slope of the linear plot for the most probable Z versus A mentioned at the beginning of this section and shown in Fig. 18. The value of S was found to be 0.467. Having fixed this quantity, the remaining paramaters P, Q, and R were obtained by fitting the data by the method of least squares to the above equation. This gave the values

$$P = 0.0528,$$
$$Q = -0.0168,$$
$$R = 1.47.$$

These values are consistent with the systematics for the parameters established by Rudstam. The final general expression for the cross section of any of the isotopes included in the analysis is

$$\ln \sigma\,(A,Z) = 0.0528\,A + 0.0168 - 1.47\,(Z - 0.467\,A)^2. \qquad (17)$$

Table III shows the comparison of the cross sections calculated from this formula with those actually measured for the 44 nuclides used. For

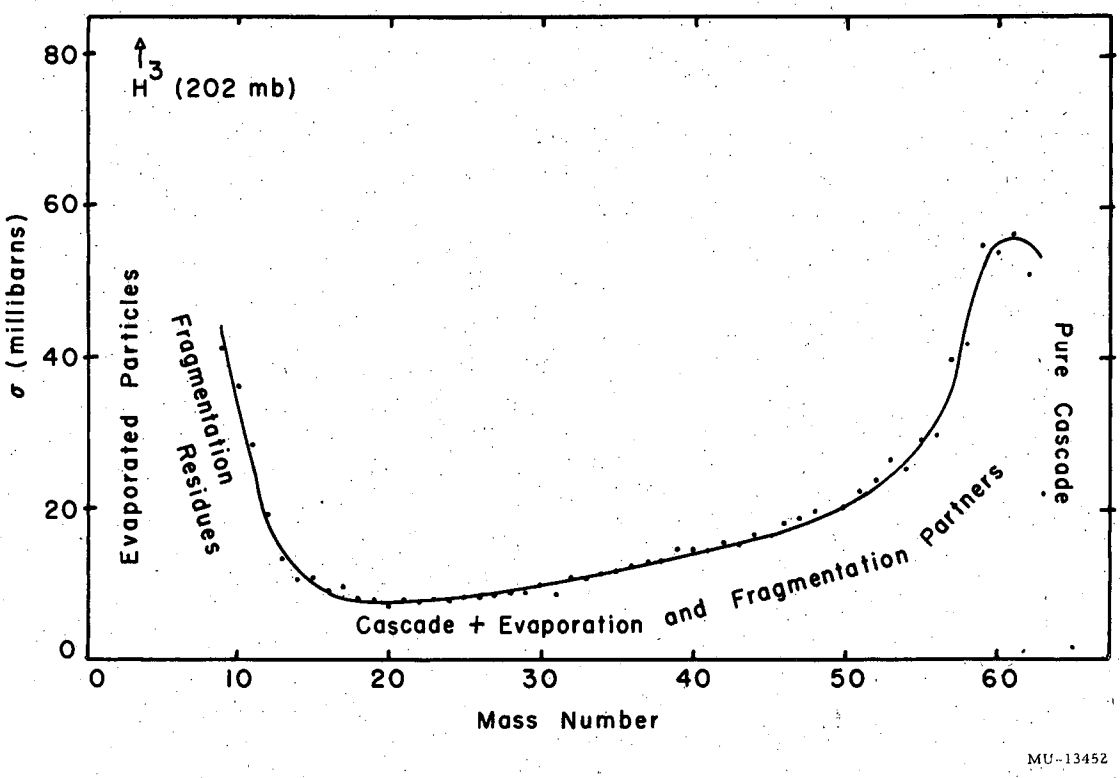

Fig. 19. Integrated isobaric cross section as a function of mass number for nuclides formed in the 5.7-Bev proton bombardment of copper.

Table III. Comparison of calculated and measured cross sections.

Nuclide	Cross Section Predicted	Cross Section Measured	Nuclide	Cross Section Predicted	Cross Section Measured
Cu^{61}	17.4	15	V^{49}	13.3	13
Cu^{60}	5.9	3.0	Ti^{45}	2.6	3.3
Ni^{57}	1.3	0.72	Sc^{43}	2.9	3.8
Co^{55}	1.5	1.8	Sc^{44}	7.7	9.3
Co^{56}	6.8	5.1	Sc^{46}	8.2	7.8
Co^{57}	16.7	24	Sc^{47}	3.2	3.0
Co^{58}	21.6	33	Sc^{48}	0.68	0.38
Co^{60}	5.3	14	Ca^{45}	2.4	1.2
Co^{61}	1.0	5.3	Ca^{47}	0.047	0.086
Fe^{52}	0.21	0.13	K^{42}	5.4	5.4
Fe^{53}	1.7	1.3	K^{43}	1.8	1.1
Fe^{55}	16.1	17	A^{37}	3.4	5.9
Fe^{59}	0.67	0.77	A^{41}	1.3	0.87
Mn^{51}	1.9	2.2	Cl^{38}	3.3	2.0
Mn^{52}	7.5	7.1	Cl^{39}	0.92	0.50
Mn^{54}	16.4	16	S^{35}	5.4	2.0
Mn^{56}	2.8	2.8	P^{32}	5.5	7.8
Cr^{48}	0.32	0.22	P^{33}	4.5	2.2
Cr^{49}	2.2	2.8	Si^{31}	3.8	2.9
Cr^{51}	14.3	14	Mg^{28}	0.82	0.65
V^{47}	2.4	3.1	Na^{22}	1.5	2.9
V^{48}	7.8	10	Na^{24}	3.4	4.8

isotopes close to the target, the predicted values are not quite so good as those more distant, but in general, the agreement is satisfactory. A graphical presentation of these data shown in Fig. 20 gives a good visual impression of the accuracy of the fit. It utilizes the fact that a plot of the quantities $\ln\sigma - PA + Q$ versus $Z - SA$ should be parabolic, as seen from Eq. (16). Finally, the root-mean-square error of the logarithms of the cross sections was calculated as $m = 0.501$. The quantity

$$\exp^{\pm m} = 1.65$$

gives the average ratio between experimental and calculated cross sections and is thus a measure of the success of the formula (17). By omitting from the analysis a few cross sections for elements close to the target (specifically the cross sections for the isotopes of copper, nickel, and cobalt), the latter figure could be lowered appreciably, which would indicate a better fit. However, an empirical formula like Eq. (17) is more useful when it covers as wide a range of mass numbers as possible.

C. Reaction Mechanisms—Comparison with Monte Carlo Predictions

The shape of the yield-mass curve of Fig. 19 reflects the processes that occur when 5.7-Bev protons strike copper nuclei. The following discussion of the present ideas on high-energy nuclear reactions is pointed toward explaining this distribution of products.

The first stage in the sequence of events that occur in a high-energy nuclear reaction is the transfer of energy by the incoming particles to the target nuclei. According to the ideas of Serber,[57] this transfer takes place by means of collisions between the projectile and individual nucleon in the target nucleus. The result is the generation of a nucleon cascade, which occurs in essentially the time it takes for the projectile to traverse the nucleus, about 10^{-22} second. The knock-on protons and neutrons which escape from the nucleus have a continuous distribution of kinetic energies up to that of the original incident particle, leaving a wide range of excitation energies in the residual nuclei, and their angular distributions are strongly peaked in the forward direction. Goldberger[58] has treated this cascade or knock-on model quantitatively, using a Monte Carlo technique. Bernardini[59] and several other workers have measured angular and energy distributions of cascade nucleons, which are in satisfactory agreement with the calculated predictions.

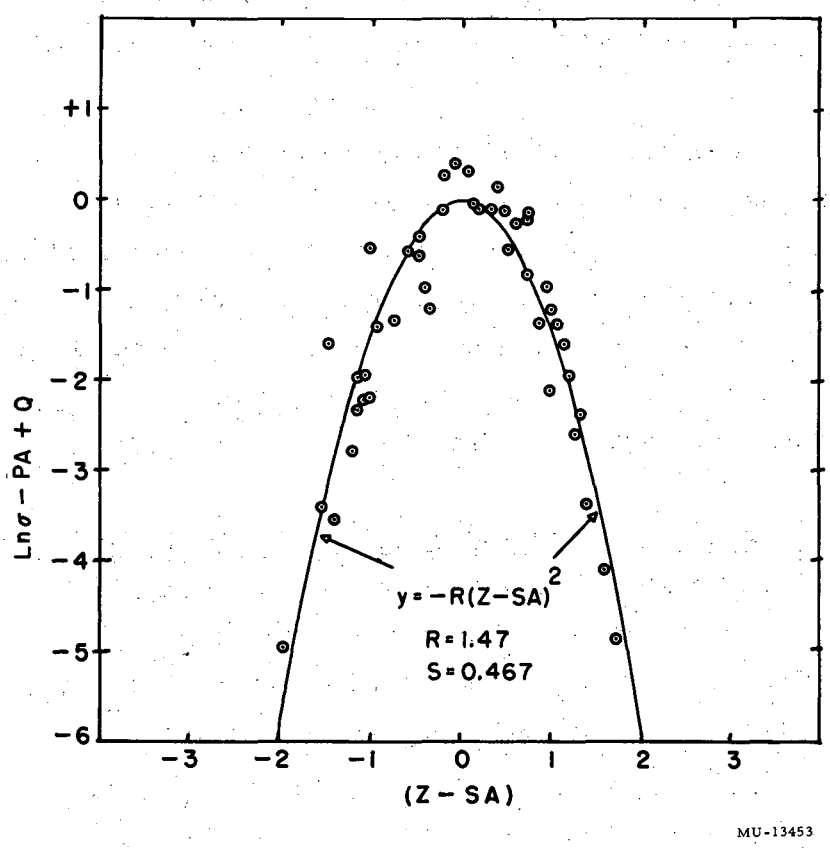

Fig. 20. Graphical presentation of experimental data fit to Eq. (17). ⊙ = experimental points.

Below about 400 Mev, where meson production is insignificant, the excited residual nuclei resulting from the fast cascade process then pass into the second stage of the reaction, which is a relatively slow dissipation of the excitation energy by evaporation of neutrons, protons, and light particles such as deuterons, tritons, alphas, and helium-3 nuclei. Quantitative calculations of the evaporation process are based on the treatments by Weisskopf,[60,61] and Le Couteur.[62] Rudstam[63] has obtained good agreement between radiochemically measured cross sections for 170-Mev protons on arsenic and calculations based on the cascade-followed-by-evaporation model, utilizing the Monte Carlo method for both stages of the reaction. He also introduces the idea of a combined cascade-compound-nucleus picture for the first step of the reaction.

Recently, G. Friedlander of Brookhaven National Laboratory, J. Miller of Columbia University, N. Metropolis, R. Bivins, and M. Storm of the Los Alamos Scientific Laboratory, and A. Turkevich of the University of Chicago have set up an extensive program for making cascade calculations using the Monte Carlo technique.[64] The essentials of the calculation have been computer-programmed so that the particle energy and target element may be varied. This enables many more initial events to be followed, leading to smaller statistical errors on the results than had previously been practical by hand calculations. The writer is indebted to Dr. A. Turkevich for making some of the preliminary results of their calculations available. Their predicted yield-mass curve for 360-Mev protons on copper is compared with that constructed from the data of Batzel[6] for 340-Mev protons (these data were corrected where necessary for better-known decay schemes) in Fig 21 (a). The agreement is very good. Although these calculations have not yet been carried out for 6-Bev protons on copper, it is interesting to compare the 2-Bev proton predictions with the results of this study, for the measured cross sections do not differ markedly from those of Friedlander[65] for 2.2-Bev protons on copper. Figures 22 (a) and 22 (b) show the frequency distribution and average excitation energies respectively of the residual nuclides resulting from the cascade process. The application of a crude evaporation calculation leads to a predicted yield-mass curve, which is compared with that found in this study in Fig. 21 (b). In this case, the agreement is not so good as that found at the lower energy, and it would

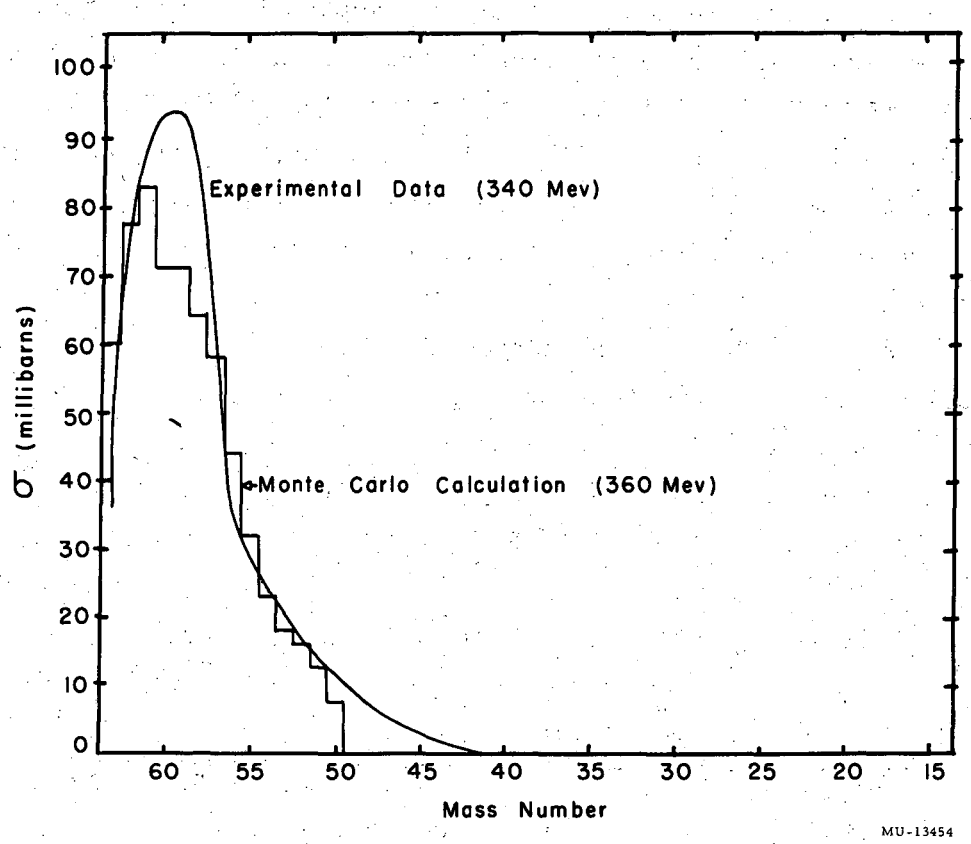

Fig. 21(a). Comparison of the experimental yield-mass distribution for 340-Mev protons on copper with the Monte Carlo prediction for this energy.

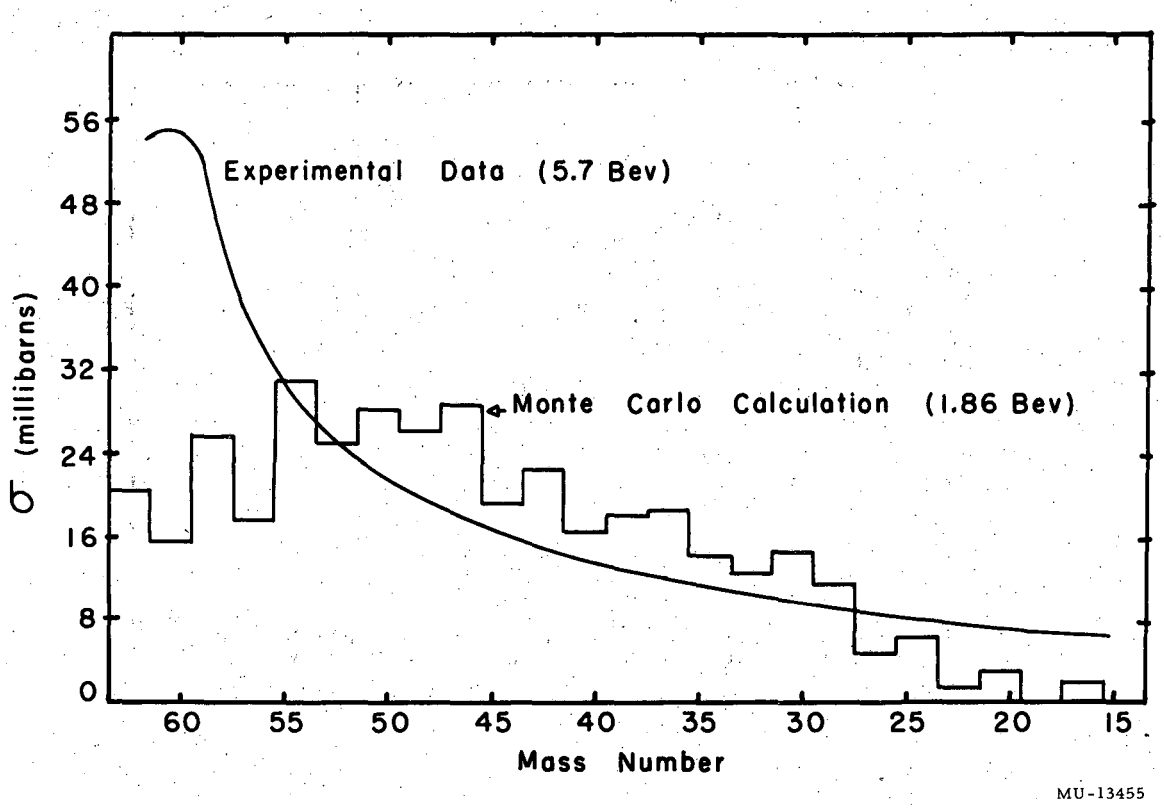

Fig. 21(b). Comparison of the experimental yield-mass distribution for 5.7-Bev protons on copper with Monte Carlo prediction for 1.86-Bev protons on copper.

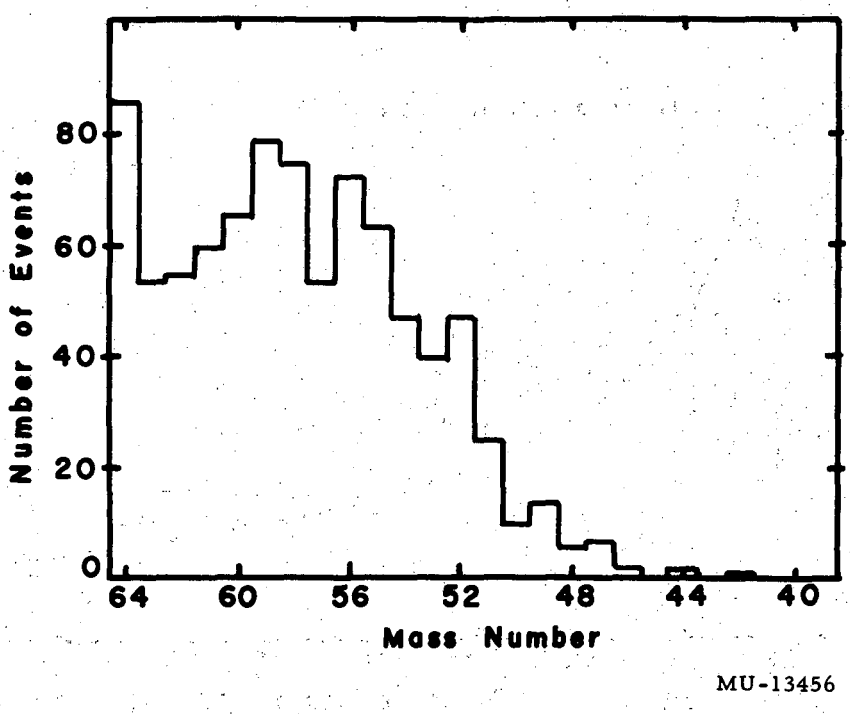

Fig. 22(a). Frequency distribution of residual nuclides after the cascade process in the 1.86-Bev proton bombardment of copper (Monte Carlo prediction).

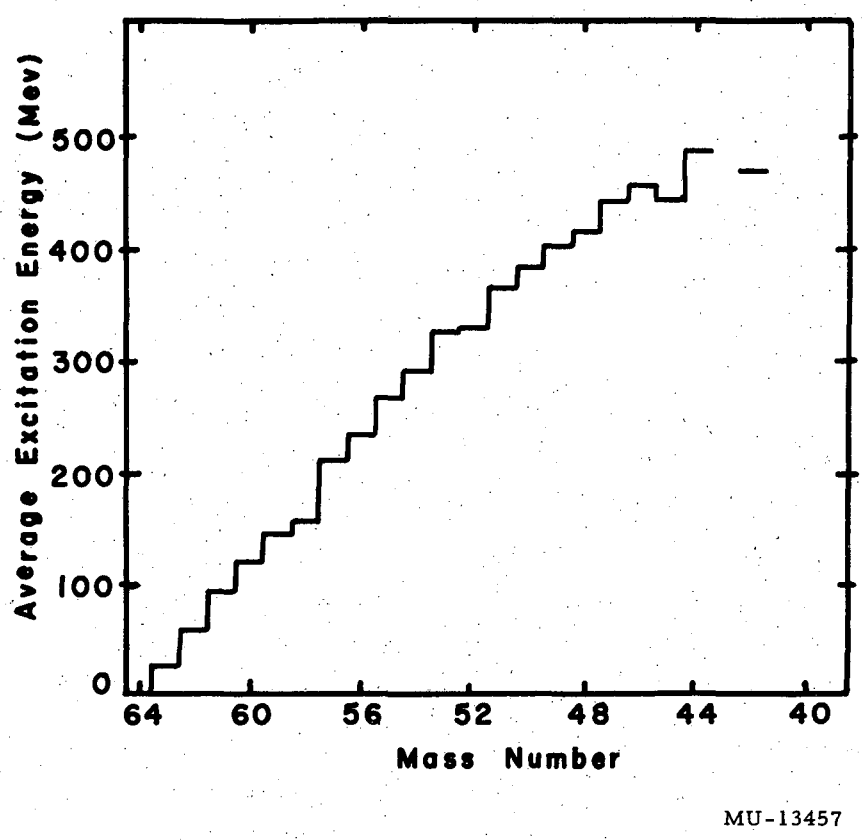

Fig. 22(b). Average excitation energies of residual nuclides after the cascade process in the 1.86-Bev proton bombardment of copper (Monte Carlo prediction).

be expected to be even less if the comparison were with 6-Bev calculations. The cascade process has evidently been overestimated in the Bev region. The eventual publication of the details of the Monte Carlo cascade calculations used for making the above comparison, especially the assumptions regarding meson participation, may suggest a reason for the discrepancy. One conceivably could account for the high yields of products close to the target (which are observed experimentally but not predicted by the 2-Bev calculations) by including in the calculations a nucleon density distribution extending outwards from the nucleus, which is a more realistic picture than the present model of a square-well potential containing the degenerate Fermi gas. A density distribution would enhance the probability of surface reactions with small energy transfer, which would lead to products close to the target. Another possibility for the discrepancy may lie in the following description of a newly observed mechanism that accompanies the onset of meson production and certainly operates for proton energies in the Bev range.

Wolfgang et al.,[66] in bombarding lead with protons in the Bev energy range, have introduced the term "fragmentation" to account for the formation of products that require large amounts of excitation energy and exhibit steeply rising excitation functions above 0.4 Bev. They describe the process in terms of the production and reabsorption of π mesons, leading to the deposition of large amounts of excitation energy in relatively small zones of the nucleus. This results in the emission of light fragments of nuclear matter in a time short compared with the life of a compound nucleus. Since it is a fast process, like the cascade, the emitted fragments initially have a neutron-to-proton ratio essentially the same as that of the target nucleus. The fragmented products then de-excite by the evaporation process. The data herein are consistent with this idea. The increase with lower mass number that starts at about A = 20 in the yield-mass curve can be explained by assuming these products are fragmentation residues. There are of course products which are the partners of the fragmented units that have also dissipated their excitation energies by evaporation; their distribution increases with larger mass number. This distribution is mixed up with the straight cascade-evaporation residues described previously. The cutoff at very low mass number between evaporated particles and fragmented ones is not clear-cut. There

is undoubtedly a continuous gradation in both mass yield and time scale between slow evaporation and fast fragmentation.

The possibility of a fission contribution to the yields of products centering around mass number 30 cannot be ruled out. In the light of the previous discussion, the fission process would differ from fragmentation only in the time scale for these events. Actual fission as such would be a slow process preceded by compound-nucleus formation. The data of Batzel indicate that this can occur,[10] but it is probably unimportant in the bombardment of copper at these energies.

In summary, the yield-mass curve observed in this work is the summation of products resulting from the following reaction mechanisms:

Step 1: Energy transfer by a nucleon cascade process and reabsorption of π-mesons produced.

Step 2: De-excitation of the residual nuclei by either

a. Spallation or slow evaporation of particles, or

b. Fragmentation or fast emission of light fragments followed by evaporation from the fragment and its partner.

The yield-mass curve of Fig. 19 has been labeled in terms of the regions of products resulting from each of these mechanisms.

D. Total Absorption Cross Section—Estimate of r_o

A summation of the experimental and interpolated cross sections over the appropriate mass numbers will yield a total absorption cross section for the bombardment of copper with 5.7-Bev protons. An examination of the yield-mass curve (Fig. 19) with an insight into the mechanisms involved indicates that the summation should properly be carried out from about mass 20 up through mass 65, excluding the gallium yields. Summing in this manner will insure as closely as possible that each event is counted only once. The result of this summation is 893 millibarns, of which 318 millibarns, or 36% of the total, is represented by directly measured yields. For comparison, if the summation is carried out from mass number 30 through mass number 65, the result is 810 millibarns. Taking the first 893-millibarn figure and assuming that it

is a measure of the cross-sectional area of a copper nucleus, neglecting transparency, one can calculate an r_o defined by

$$R = r_o A^{1/3} \times 10^{-13} \text{ centimeters,} \tag{18}$$

where R = equivalent square-well radius of a nucleus of definite boundary having mass number A,

since we have

$$\pi R^2 = 893 \times 10^{-27} \text{ square centimeters.} \tag{19}$$

The result is

$$r_o = 1.33.$$

Sinha and Das[67] have recently measured a cross section for copper corresponding to the distance at which nuclear forces are effective, using cosmic-ray interactions of 4 Bev average energy. Their result was 899 millibarns and an r_o of 1.34.

As a function of particle energy, the absorption cross section for protons or neutrons on copper passes through a shallow minimum in the hundreds-of-Mev energy range,[68] owing to the phenomenon of nuclear transparency interpreted in terms of the optical model of the nucleus.[69] However, ultra-high-energy cosmic-ray data indicate that it rises again to the geometric value, presumably because of an increase in the elementary nucleon-nucleon cross sections.[70,71] The result in this work is consistent with this trend, but it is somewhat higher than other estimates of the absorption cross section for accelerator particles in the Bev energy range.[72] This may be due to the difficulty of deciding on a low-mass-number cutoff for the summation.

E. Observations on Some Specific Reactions of Interest

1. Difference in (p,pn) Yields

The formation cross sections for Cu^{64} and Cu^{62} represent (p,pn) or equivalent reactions on the two stable isotopes of natural copper, which have mass numbers 63 and 65 with natural abundances of 69% and 31% respectively. Assuming that the (p,p3n) reaction on Cu^{65}, which can also form Cu^{62}, is negligible compared with its (p,pn) contribution, the observed cross sections for Cu^{64} and Cu^{62} may be weighted by the isotopic abundances of natural copper to give a pair of (p,pn) figures, which may

be compared in order to see if there is any mass effect in this elementary reaction. The results are

$$(p,pn)_{Cu^{63}} = 46 \text{ millibarns}, \qquad (p,pn)_{Cu^{65}} = 71 \text{ millibarns}.$$

Markowitz[73] has measured the excitation functions for these reactions, both with separated isotopes and with natural copper targets, and has found them to be quite flat in the Bev energy region. At 3.0 Bev, he found a value of 66 millibarns for Cu^{63} (p,pn) Cu^{62}, although in some runs his determinations were as low as that found above. Since Cu^{62} is a 10-minute activity, experimental difficulties make the determination of its cross section much less accurate than that of 13-hour Cu^{64}, for which he obtains values in excellent agreement with those found in this work. In order to insure an overlap of energies, two Bevatron bombardments were carried out at 2.2 Bev in which copper was removed. The average result for Cu^{64} based on the isotopic abundance of stable Cu^{65} was 61 millibarns, which verifies the observations by Markowitz that this (p,pn) cross section is essentially constant in the Bev energy range, although there may be a slight rise in going from 2 to 6 Bev.

However, if the above difference in (p,pn) yields found here is actually real, it could be explained by assuming that the extra pair of neutrons in Cu^{65} is "concentrated" toward the surface of the nucleus, where cascade collisions leading to this reaction are most likely to occur. This idea of a neutron "skin" type of distribution in nuclei was first proposed by Johnson and Teller.[74] Wilets,[75] on the other hand, has concluded that the density distributions in nuclei are about the same for neutrons and protons, although his calculations do indicate that the tail of the neutron distribution extends beyond that for protons. Thus, it is conceivable that the excess of neutrons in Cu^{65} over Cu^{63} would tend to participate in surface reactions like the (p,pn), leading to a larger cross section in Cu^{65}. The reaction is interesting enough to warrant further study in order to ascertain whether or not the difference in yields is actually outside experimental error.

2. Cu^{65} $(p,p\pi^+)$ Ni^{65}

The cross section for formation of Ni^{65} in the proton bombardment of Cu^{65} has been studied by Fung and Turkevich[76] up to 440 Mev. They concluded that this product is due to a reaction involving the production of positive pions according to the collision reaction

$$p + (p) \longrightarrow p + n + \pi^+,$$

where (p) refers to a proton bound in the nucleus. Therefore, one might expect that the excitation function for this reaction would resemble that for the production of mesons through proton-proton collisions, which rises rapidly above the meson-production threshold to a value of about 28 millibarns at 1 Bev, after which it remains constant out to 6 Bev. Correspondingly, the above reaction has a threshold around 200 Mev, and the cross section increases rapidly to 0.083 millibarn at 440 Mev. The value found in this work at 5.7 Bev is 0.22 millibarn. In addition, the data of Nethaway[56] on In^{115} $(p,p\pi^+)$ Cd^{115} show that the cross section for this reaction remains constant from 2 to 6 Bev at 0.21 millibarn. Thus, the shape of the energy dependence of the cross section is consistent with the interpretation of this reaction in terms of the meson process described.

3. Secondary-Product Yields

The observed yields of gallium isotopes are attributed to the interactions of secondary helium nuclides with target nuclei. These secondary particles may be ejected fragments resulting from the initial cascade step, or evaporated particles of lower energy, in which case they are probably not nearly as effective as the former in producing further reactions with copper nuclei. Turkevich and Sugarman[77] have studied this effect, using 2.2-Bev protons on copper, and they observed product yields up to arsenic corresponding to secondary beryllium reactions. In order to gain any kind of useful information from a secondary-product study, it is necessary to bombard thick and thin foils and note the change in effective cross sections with target thickness. This information allows an estimate of the reaction distances of the fragments and their average energies. The number of these fragments reacting per proton-copper interaction can then

be calculated by use of low-energy excitation functions for the appropriate particle, such as those of Porges[78] for alphas on copper to give the gallium isotopes. The results obtained in this study were on 3-mil copper foils, and simply indicate that nothing anomalous occurred with respect to these secondary-product yields in going from 2 to 6 Bev.

4. Differences in Yields of Isomers

The ratio of yields for a pair of isomers of a nuclide formed in target bombardments may be of significance in determining the effects introduced by states of different angular momentum. For example, a residual nucleus from the cascade process containing a large amount of excitation energy presumably has a high spin also, and may tend to retain this state while de-exciting by evaporation, leading to preferential formation of the high spin state of an isomeric pair. On the other hand, the evaporated particles, although of low energy, may carry off most of the angular momentum, leading to low-spin-state preference in isomers. There is actually no good theory at present on how these yields should vary with distance from the target nucleus and with incident-particle energy. The results found in this work are summarized:

Nuclide	Total Angular Momentum, J	Cross Section (mb)
Mn^{52m}	2 $\hbar$	1.9
Mn^{52}	6 $\hbar$	5.2
Sc^{44m}	6, 7 $\hbar$	4.7
Sc^{44}	2, 3 $\hbar$	4.6
Cl^{34m}	3 $\hbar$	0.73
Cl^{34}	0 $\hbar$	0.92

The Cl^{34} ground-state cross section is estimated from the measured value for the isomer and from the total Cl^{34} yield obtained through interpolation methods. These data indicate that there is a definite discrimination toward the high spin state exhibited in Mn^{52} that is not apparent for the other two isotopes formed.

ACKNOWLEDGMENTS

I want to express my gratitude to Professor Glenn T. Seaborg, under whose guidance this work was performed, and to Dr. Earl K. Hyde and Dr. Lester Winsberg for their interest and helpful advice. I would also like to thank Dr. Albert Caretto, Dr. Rex Shudde, Mr. Paul Benioff, and Mr. James Grover for many valuable discussions on certain phases of this work. In addition, my most sincere thanks are extended to Dr. Edward Lofgren and the Bevatron operating group for their co-operation; to George Shalimoff for the spectrographic analyses of the target materials; to Dr. William Wade for assistance in obtaining the tritium and argon samples; to Dr. Albert Caretto for his data on fluorine-18 from copper; and to Dr. Eugene Huffman, Eugene Lee, Edward Jeung, and Karl Marhenke for the chemical analyses of many samples.

This work was performed under the auspices of the United States Atomic Energy Commission.

APPENDICES

A. Traversals as a Function of Target Thickness

The following is a derivation of the number of traversals the proton beam makes through a foil stack in terms of the shrinkage of the proton orbit due to energy loss in the foils and the variation of the magnetic field with time. It has been derived by Mr. Paul Benioff, to whom the writer expresses his thanks for allowing its reproduction here.

Let $r = f(T,t)$,

where r = radius of proton orbit,

T = kinetic energy of protons,

t = time.

Writing the total differential, we have

$$dr = \frac{\partial r}{\partial T} dT + \frac{\partial r}{\partial t} dt, \tag{A.1}$$

since $$Hev = \frac{Mv^2}{r} ; \tag{A.2}$$

therefore, we have

$$r = \frac{Mv}{He} , \tag{A.3}$$

where M = mass of proton at velocity v,

H = magnetic field,

e = electronic charge.

The relativistic momentum as a function of the kinetic energy of the protons is given by

$$Mv = \frac{(T^2 + 2M_o c^2 T)^{1/2}}{c} , \tag{A.4}$$

where M_o = rest mass of proton,

c = velocity of light.

Substituting Eq. (A.4) into (A.3), one obtains

$$r = \frac{(T^2 + 2M_o c^2 T)^{1/2}}{Hec} . \tag{A.5}$$

In addition, the magnetic field varies with radius according to

$$H_{(r)} = H_{(r_o)} \left(\frac{r_o}{r}\right)^m , \tag{A.6}$$

where m = a constant for the Bevatron.

Substituting Eq. (A.6) into (A.5) and evaluating the partial of r with respect to T yields

$$\frac{\partial r}{\partial T} = \frac{r_o \, (T + M_o c^2)}{(1-m) \, (T^2 + 2M_o c^2 T)} . \tag{A.7}$$

Also,

$$dT = \frac{dE}{dX} \, bn, \tag{A.8}$$

where $\frac{dE}{dX}$ = rate of proton energy loss with target thickness,

b = thickness of foil,

n = number of traversals.

Inserting Eqs. (A.7) and (A.8) into (A.1) gives

$$dr = \frac{r_o \, (T + M_o c^2)}{(1-m) \, (T^2 + 2M_o c^2 T)} \, \frac{dE}{dX} \, bn + \frac{\partial r}{\partial t} \, dt. \tag{A.9}$$

Now, the variation of magnetic field with time is such that we have

$$\frac{\partial r}{\partial t} = \text{constant} = \frac{1 \text{ inch}}{1.60 \text{ milliseconds}} \tag{A.10}$$

and

$$dt = \frac{n}{f}, \tag{A.11}$$

where f = proton rotation frequency.

Since the relation is

$$\overline{f} = \frac{4 \times 10^6 \text{ revolutions}}{1.8 \text{ seconds}} ,$$

then we have

$$\frac{\partial r}{\partial t} \, dt = 0.0003 \, n \text{ inch}. \tag{A.12}$$

Substituting Eq. (A.12) into (A.9) and using the following values for the constants in Eq. (A.9) leads to these final results:

r_o = 600 inches,
T = 5,700 Mev,
$M_o c^2$ = 938 Mev,
m = 0.6,

$$dr = \Delta r = (0.220 \frac{dE}{dX} b + 0.0003) n. \qquad (A.13)$$

Eq. (A.13) is discussed in Section I of the main text.

B. Least-Squares Analysis

Applied to a Two-Component Radioactive Decay System

The following application of the least-squares method of analysis to a two-component decay system serves as an illustration of the general principles involved in the use of this method. The total activity in a system containing two separate radioactive components which are decaying is given by

$$A = A_1^o e^{-\lambda_1 t} + A_2^o e^{-\lambda_2 t}, \qquad (B.1)$$

A = total activity,
A_1^o = activity of component 1 at end of bombardment,
A_2^o = activity of component 2 at end of bombardment,
λ_1, λ_2 = decay constants of components 1 and 2 respectively,
t = time measured from end of bombardment.

The residual x is defined by

$$A - A_1^o e^{-\lambda_1 t} - A_2^o e^{-\lambda_2 t} = x. \qquad (B.2)$$

By definition, the method of least squares minimizes the sum of the squares of the residuals. Therefore, the first step is to square and sum the residuals defined in Eq. (B.2):

$$\sum_i x_i^2 = \sum_i (A_i^2 - 2A_i A_1^o e^{-\lambda_1 t} - 2A_i A_2^o e^{-\lambda_2 t} + 2A_1^o A_2^o e^{-t(\lambda_1+\lambda_2)} + A_1^{o\,2} e^{-2\lambda_1 t} + A_2^{o\,2} e^{-2\lambda_2 t}. \qquad (B\text{-}3)$$

Next, minimizing this sum by taking its partial derivative with respect to the two parameters being sought, namely A_1^o and A_2^o, and setting these differentiations equal to zero, gives the following pair of simultaneous equations:

$$\frac{\partial \sum_i x^2}{\partial A_1^o} = 0 = \sum_i \left(-2A_i e^{-\lambda_1 t} + 2A_2^o e^{-t(\lambda_1+\lambda_2)} + 2A_1^o e^{-2\lambda_1 t}\right), \tag{B.4}$$

$$\frac{\partial \sum_i x^2}{\partial A_2^o} = 0 = \sum_i \left(-2A_i e^{-\lambda_2 t} + 2A_1^o e^{-t(\lambda_1+\lambda_2)} + 2A_2^o e^{-2\lambda_2 t}\right). \tag{B.5}$$

Solving this last pair simultaneously leads to the results

$$A_1^o = \frac{\sum_i A_i e^{-\lambda_2 t} \sum_i e^{-t(\lambda_1+\lambda_2)} - \sum_i A_i e^{-\lambda_1 t} \sum_i e^{-2\lambda_2 t}}{\left[\sum_i 2^{-t(\lambda_1+\lambda_2)}\right]^2 - \sum_i e^{-2\lambda_1 t} \sum_i e^{-2\lambda_2 t}}, \tag{B.6}$$

$$A_2^o = \frac{\sum_i A_i e^{-\lambda_1 t} - A_1^o \sum_i e^{-2\lambda_1 t}}{\sum_i e^{-t(\lambda_1+\lambda_2)}}. \tag{B.7}$$

Experimental data may be set up in the following table for evaluation of the quantities necessary for calculating A_1^o and A_2^o :

Item No.	1	2	3	4[a]	5	6[b]	7[c]	8[d]	9[e]
	t	A_i	$e^{-\lambda_1 t}$	$e^{-2\lambda_1 t}$	$e^{-\lambda_2 t}$	$e^{-2\lambda_2 t}$	$A_i e^{-\lambda_1 t}$	$A_i e^{-\lambda_2 t}$	$e^{-t(\lambda_1+\lambda_2)}$
				$\sum$		$\sum$	$\sum$	$\sum$	$\sum$

[a]Product of item 3 times item 3.

[b]Product of item 5 times item 5.

[c]Product of item 2 times item 3.

[d]Product of item 2 times item 5.

[e]Product of item 3 times item 5.

Finally, using the summations for the respective columns, one obtains

$$A_1^o = \frac{(8)\,(9) - (7)\,(6)}{(9)^2 - (4)\,(6)}, \tag{B.8}$$

$$A_2^o = \frac{(7) - A_1^o\,(4)}{(9)}. \tag{B.9}$$

REFERENCES

1. D. Templeton, Annual Review of Nuclear Science 2, 93 (1953).
2. G. Rudstam, Phil. Mag. 46, 344 (1955).
3. Rex H. Shudde, Fission of Uranium with 5.7-Bev Protons (Thesis), UCRL-3419, June 1956.
4. I. Halpern, Mass. Inst. of Tech. Report, 1953; Debs, Eisinger, Fairhall, Halpern, and Richter, Phys. Rev. 97, 1325 (1955).
5. Bartell, Helmholz, Softky, and Stewart, Phys. Rev. 80, 1006 (1950).
6. Batzel, Miller, and Seaborg, Phys. Rev. 84, 671 (1951).
7. Miller, Thompson, and Cunningham, Phys. Rev. 74, 347 (1948).
8. Vinogradov, Alimarin, Baranov, Lavrukhina, Baranova, and Pavlotskaya, Session of the Academy of Sciences of the U.S.S.R. on the Peaceful Uses of Atomic Energy, July 1955 (English translation), p. 85.
9. L. Marquez, Phys. Rev. 88, 225 (1952).
10. R. Batzel and G. T. Seaborg, Phys. Rev. 82, 607 (1951).
11. L. Marquez, Phys. Rev. 86, 405 (1952).
12. D. Greenberg and J. M. Miller, Phys. Rev. 84, 845 (1951).
13. N. Bohr, Nature 137, 344 (1936).
14. S. Fung and I. Perlman, Phys. Rev. 87, 623 (1952).
15. R. Wolfgang and G. Friedlander, Phys. Rev. 94, 775 (1954).
16. M. Livingston, Annual Review of Nuclear Science 1, 169 (1952).
17. M. Rich and R. Madey, Range-Energy Tables, UCRL-2301, March 1954, p. 39.
18. Currie, Libby, and Wolfgang, Phys. Rev. 101, 1558 (1956).
19. R. Wolfgang and G. Friedlander, Phys. Rev. 96, 190 (1954).
20. Friedlander, Hudis, and Wolfgang, Phys. Rev. 99, 263 (1955).
21. Crandall, Millburn, Pyle, and Birnbaum, Phys. Rev. 101, 329 (1956).
22. Hicks, Stevenson, and Nervik, Phys. Rev. 102, 1390 (1956).

23. Cumming, Swartz, and Friedlander, Bull. Am. Phys. Soc. 1 (4), 225 (1956).

24. Horwitz, Murray, and Crandall, Bull. Am. Phys. Soc. 1 (4), 225 (1956).

25. Nahmin Horwitz, UCRL, private communication.

26. R. Duffield and N. Sugarman, Phys. Rev. 94, 776 (1954).

27. Lester Winsberg, UCRL, private communication.

28. W. Wayne Meinke, Chemical Procedures Used in Bombardment Work at Berkeley, UCRL-432 (now AECD-2738), August 1949.

29. Manfred Lindner, Radiochemical Procedures in Use at the University of California Radiation Laboratory (Livermore), UCRL-4377, Aug. 1954.

30. Jacob Kleinberg, Collected Radiochemical Procedures, LA-1566, Sept. 1953.

31. H. Finston and J. Miskel, Annual Review of Nuclear Science 5, 278 (1955).

32. Lloyd R. Zumwalt, U. S. Atomic Energy Commission Unclassified Report AECU-567, Sept. 1949.

33. B. Burtt, Nucleonics 5, 28 (1949).

34. Gleason, Taylor, and Tabern, Nucleonics 8, 12 (1951).

35. H. Seliger, Phys. Rev. 88, 408 (1952).

36. H. Seliger, Phys. Rev. 78, 491 (1950).

37. W. Nervik and P. Stevenson, Nucleonics 10, 18 (1952).

38. G. Friedlander and J. Kennedy, Nuclear and Radiochemistry (Wiley, New York, 1955), p. 295-296.

39. Way, King, McGinnis, and van Lieshout, Nuclear Level Schemes, TID-5300, June 1955.

40. F. Ajzenberg and T. Lauritsen, Revs. Modern Phys. 27, 77 (1955).

41. P. Endt and J. Kluyver, Revs. Modern Phys. 26, 95 (1954).

42. M. I. Kalkstein and J. M. Hollander, A Survey of Counting Efficiencies for a 1-1/2-Inch-Diameter by 1-Inch-High Sodium Iodide (Thallium Activated) Crystal, UCRL-2764, October 1954.

43. L. Magnusson, to be published in Phys. Rev.

44. Peter Axel, Escape Peak Correction to Gamma-Ray Intensity Measurements Made with Sodium Iodide Crystals, BNL-271, September 1953.

45. C. Davisson and R. Evans, Revs. Modern Phys. 24, 79 (1952).

46. S. Allen, Handbook of Chemistry and Physics, 32nd Ed. (Chemical Rubber Publishing Co., Cleveland, 1950), p. 2181.

47. E. Burhop, The Auger Effect and Other Radiationless Transitions (Cambridge University Press, Cambridge, England, 1952).

48. Broyles, Thomas, and Haynes, Phys. Rev. 89, 715 (1953).

49. M. Studier and R. James, UCRL, unpublished work (1946).

50. D. Nethaway and A. Caretto, UCRL, private communication.

51. Penning, Maltrud, Hopkins, and Schmidt, Phys. Rev. 104, 740 (1956).

52. van Lieshout, Greenberg, and Wu, Phys. Rev. 98, 1171A (1955).

53. J. Wilkinson and R. Sheline, Phys. Rev. 98, 1538A (1955); Phys. Rev. 99, 165 (1955).

54. C. Sharp Cook and F. Tomnovec, Phys. Rev. 104, 1407 (1956).

55. A. Pappas, Fra Fysikkens Verden 16, 161 (1954).

56. David R. Nethaway, Excitation Functions for Reactions of Bev Protons on Indium (Master's Thesis), UCRL-3628, January 1957.

57. R. Serber, Phys. Rev. 72, 1114 (1947).

58. M. Goldberger, Phys. Rev. 74, 1269 (1948).

59. Bernardini, Booth, and Lindenbaum, Phys. Rev. 85, 826 (1952); Phys. Rev. 88, 1017 (1952).

60. V. Weisskopf, Phys. Rev. 52, 295 (1937).

61. J. Blatt and V. Weisskopf, Theoretical Nuclear Physics (Wiley, New York, 1952), Chapter VIII.

62. K. Le Couteur, Proc.Roy.Soc. (London) 63 A, 259 (1950); ibid. 65 A, 718 (1952).

63. Gösta Rudstam, Spallation of Medium Weight Elements (Thesis), Uppsala, November 1956.

64. Friedlander, Miller, Metropolis, Bivins, Storm, and Turkevich, Bull. Am. Phys. Soc. 2, (No. 1), 63 (1957).

65. Friedlander, Miller, Wolfgang, Hudis, and Baker, Phys. Rev. 94, 727 (1954).

66. Wolfgang, Baker, Caretto, Cumming, Friedlander, and Hudis, Phys. Rev. 103, 394 (1956).

67. M. Sinha and N. Das, Phys. Rev. 105, 1587 (1957).

68. Millburn, Birnbaum, Crandall, and Schecter, Phys. Rev. 95, 1268 (1954).

69. Fernbach, Serber, and Taylor, Phys. Rev. 75, 1352 (1949).

70. R. Williams, Phys. Rev. 98, 1393 (1955).

71. N. Kocharian, Doklady translation 1 (No. 2), 209 (1956).

72. Coor, Hill, Hornyak, Smith, and Snow, Phys. Rev. 98, 1369 (1955).

73. Samuel Markowitz, (p,pn) Reactions in the Bev Energy Range (Thesis), Princeton University, January 1957.

74. M. Johnson and E. Teller, Phys. Rev. 93, 357 (1954).

75. L. Wilets, Phys. Rev. 101, 1805 (1956).

76. S. Fung and A. Turkevich, Phys. Rev. 95, 176 (1954).

77. A. Turkevich and N. Sugarman, Phys. Rev. 94, 728 (1954).

78. K. Porges, Phys. Rev. 101, 225 (1956).